

Simulating spin-boson models with trapped ions

A. Lemmer,^{1,*} C. Cormick,² D. Tamascelli,^{1,3} T. Schaetz,⁴ S. F. Huelga,¹ and M. B. Plenio^{1,†}

¹*Institut für Theoretische Physik and IQST, Universität Ulm, Albert-Einstein Alle 11, 89069 Ulm, Germany*

²*IFEG, CONICET and Universidad Nacional de Córdoba, X5000HUA, Córdoba, Argentina*

³*Dipartimento di Fisica, Università degli Studi di Milano, Via Celoria 16, 20133 Milano, Italy*

⁴*Physikalisches Institut, Albert-Ludwigs-Universität Freiburg, Hermann-Herder-Str.3, 79104 Freiburg, Germany*

(Dated: February 28, 2022)

We propose a method to simulate the dynamics of spin-boson models with small crystals of trapped ions where the electronic degree of freedom of one ion is used to encode the spin while the collective vibrational degrees of freedom are employed to form an effective harmonic environment. The key idea of our approach is that a single damped mode can be used to provide a harmonic environment with Lorentzian spectral density. More complex spectral functions can be tailored by combining several individually damped modes. We propose to work with mixed-species crystals such that one species serves to encode the spin while the other species is used to cool the vibrational degrees of freedom to engineer the environment. The strength of the dissipation on the spin can be controlled by tuning the coupling between spin and vibrational degrees of freedom. In this way the dynamics of spin-boson models with macroscopic and non-Markovian environments can be simulated using only a few ions. We illustrate the approach by simulating an experiment with realistic parameters and show by computing quantitative measures that the dynamics is genuinely non-Markovian.

The spin-boson model is an archetypical model of an open quantum system with applications ranging from chemical reactions [1] over biological aggregates [2] to solid state physics [3–5]. The model describes a single spin coupled to a dissipative environment comprised by an infinite set of harmonic oscillators. It is well known that the effect of thermal oscillator environments on a quantum system is fully described by a single scalar function, the spectral density (or spectral function) of the environment [4]. Although approximate analytic solutions have been found for some spectral densities [3, 4] no closed analytic solution of the spin-boson model is known. Meanwhile, dynamics and thermodynamical properties of spin-boson models have been investigated by a number of numerical approaches including techniques based on the numerical renormalization group [5], time-dependent density matrix renormalization group [6, 7], path integral Monte Carlo [8], or the quasi-adiabatic propagator path integral approach [9]. Numerical simulations are especially needed for environments with spectral densities where the reorganization energy is of the order of the spectral width or highly structured environments with long-lived vibrational modes that lead to highly non-trivial dynamics. These types of spectral densities are of particular relevance for the excitonic and electronic dynamics in biomolecular systems [10] and pose considerable challenges for numerical methods especially when the results of non-linear spectroscopy need to be predicted [11]. Therefore, an experimental simulator with a high degree of control is desirable.

Trapped atomic ions provide a clean and highly controllable system where many dynamical quantities are directly accessible. They have proven to be a versatile platform for the simulation of a wide range of physical models, such as defect formation in classical phase transitions [12–14] as well as open

and closed quantum systems [15–20]. The simulation of spin-boson models using trapped atomic ions has been proposed previously [21] requiring rather large crystals comprising 50–100 ions. Such crystals feature a large number of vibrational modes which can be used to act as a mesoscopic environment for the spin. However, for these large crystals the level of control needed to simulate spin-boson models is not available in the foreseeable future. In this work, we develop a proposal to simulate the dynamics of spin-boson models using small crystals of trapped ions. Our procedure also relies on the vibrational degrees of freedom to model the environment, but it makes use of the fact that a damped mode produces an effective Lorentzian spectral density [1]. While in [1] the damping is provided by an oscillator reservoir with Ohmic spectral density we show that the same spectral density can be obtained in certain regions of parameter space if the damping is modeled by a Lindblad equation extending the results of [22–25]. The resulting spectral densities are continuous functions of frequency and can thus be identified with an environment made up of a macroscopic number of modes as it occurs in the condensed phase. Controlling the couplings of the spin to the modes, the mode frequencies and the damping rates, the shape of the spectral density can be tailored, allowing one to mimic environments with continuous and highly-structured spectral densities using only a small number of oscillators to form the environment. This reduced overhead brings the simulation of spin-boson models to the realm of state-of-the-art trapped-ion setups.

Spin-boson model.— The spin-boson model describes a two-level system (spin 1/2) in a dissipative environment which is modeled by an infinite set of non-interacting harmonic oscillators. Denoting by ε the energy splitting between the spin states $|\uparrow\rangle$ and $|\downarrow\rangle$ and by $\hbar\Delta$ the coupling between them, the Hamiltonian of the global system reads [3]

$$H_{\text{sb}} = \frac{\varepsilon}{2}\sigma^z - \frac{\hbar\Delta}{2}\sigma^x - \frac{1}{2}\sigma^z \sum_n \hbar\lambda_n (a_n + a_n^\dagger) + \sum_n \hbar\omega_n a_n^\dagger a_n \quad (1)$$

where $\sigma^z = |\uparrow\rangle\langle\uparrow| - |\downarrow\rangle\langle\downarrow|$ and $\sigma^x = |\uparrow\rangle\langle\downarrow| + |\downarrow\rangle\langle\uparrow|$.

*Electronic address: andreas.lemmer@uni-ulm.de

†Electronic address: martin.plenio@uni-ulm.de

$a_n^\dagger(a_n)$ denotes the raising (lowering) operator of environmental mode n and ω_n the corresponding frequency while the real λ_n describe the couplings of the spin to the environmental oscillators. The spectral density which determines the influence of the oscillator environment on the spin [4] reads $J(\omega) = \pi \sum_n \lambda_n^2 \delta(\omega - \omega_n)$ with δ the Dirac δ -function. For a macroscopic environment one assumes that the frequencies are so closely spaced that $J(\omega)$ becomes a continuous function of ω .

One is generally interested in finding the reduced dynamics of the spin for an environment with a certain spectral density. The path-integral formalism [26] provides us with an exact expression for the propagator of the spin state where the effects of the environment are already included. For factorizing initial conditions $\rho_0 = \rho_s \otimes \rho_\beta$ with some spin state ρ_s and the environmental modes in a thermal state ρ_β at inverse temperature $\beta = (k_B T)^{-1}$ the propagator for the spin reads [27]

$$G(t, 0) = \int_{q_0}^{q_f} Dq \int_{q'_0}^{q'_f} Dq' e^{\frac{i}{\hbar}(S_0[q] - S_0[q'])} F[q, q']. \quad (2)$$

Here the path integral $\int_{q_0}^{q_f} Dq$ runs over all spin state trajectories connecting $q(0) = q_0$ and $q(t) = q_f$, $S_0[q]$ is the action of the free spin evolution and $F[q, q']$ is the Feynman-Vernon influence functional [27]. The influence functional contains the effect of the environment on the spin dynamics. For an oscillator environment and the considered coupling it can be written as [3]

$$F[q, q'] = \exp \left\{ - \int_0^t dt' \int_0^{t'} ds [q(t') - q'(t')] \right. \\ \left. [L(t' - s)q(s) - L^*(t' - s)q'(s)] \right\} \quad (3)$$

where $L(t) = \frac{1}{\hbar^2} (X(t)X(0))_\beta$ is the reservoir correlation function with $X = \sum_n \hbar \lambda_n (a_n + a_n^\dagger)$. Alternatively, $L(t)$ can be expressed in terms of the spectral density $J(\omega)$:

$$L(t) = \frac{1}{\pi} \int_0^\infty d\omega J(\omega) \left[\coth \left(\frac{\beta \hbar \omega}{2} \right) \cos(\omega t) - i \sin(\omega t) \right]. \quad (4)$$

Spectral density of damped harmonic oscillators.—The key idea of our approach is the fact that a damped oscillator provides a continuous effective spectral density, and the observation that different environments that produce the same influence functional have the same effect on the spin dynamics [27].

Let us first consider an environment consisting of a single harmonic oscillator which is damped by an oscillator reservoir with Ohmic spectral function. If we denote the free oscillation frequency of the damped oscillator by Ω and the bath causes damping at rate κ on the oscillator, the effective spectral density generated by the damped oscillator on the spin is Lorentzian [1, 28]

$$J_{\text{eff}}(\omega) = \lambda^2 \left[\frac{\kappa}{\kappa^2 + (\omega - \omega_m)^2} - \frac{\kappa}{\kappa^2 + (\omega + \omega_m)^2} \right]. \quad (5)$$

Here $\omega_m = \sqrt{\Omega^2 - \kappa^2}$ is the reduced frequency of the damped oscillator and $\hbar \lambda$ the spin-oscillator coupling as in Eq. (1).

Note that we restrict our considerations to the underdamped regime $\kappa < \Omega$.

The combined influence functional of several independent damped harmonic oscillators is given by the product of the individual influence functionals [27]. Therefore, if the reservoirs have the same temperature, according to Eqs. (3) and (4) their spectral densities add up and one can construct effective spectral densities $J(\omega) = \sum_n J_{\text{eff},n}(\omega)$. Here $J_{\text{eff},n}(\omega)$ is the spectral density due to oscillator n given by Eq. (5) with the corresponding $\lambda_n, \kappa_n, \omega_n$. If one wants to approximate a certain target spectral density $J_t(\omega)$ the values for $\lambda_n, \kappa_n, \omega_n$ are found by minimizing the functional $E[\{\lambda_n, \kappa_n, \omega_n\}] = \int_0^\infty d\omega |J_t(\omega) - J(\omega)|^2$ as has been shown in [40].

In trapped-ion experiments, the motion of the ions is usually expressed in terms of a set of normal modes, each of which is a harmonic oscillator. Cooling of the modes is commonly described by a Lindblad equation [41, 42]. Therefore, it is not immediately clear if we can obtain an effective spectral density as for the oscillator damped by an Ohmic bath, Eq. (5). We will now show that this is possible and we obtain the same spectral function for appropriate parameters.

Let us start by considering the reservoir correlation function $L(t)$ in Eq. (4). We note that $L(t) = L'(t) + iL''(t)$ is a complex-valued function with real and imaginary parts $L'(t)$ and $L''(t)$. For the oscillator damped by an Ohmic bath the coordinate correlation function and thus $L(t)$ can be calculated analytically [3, 28, 43] and we obtain $L'(t) = L_1(t) + L_2(t)$

$$L_1(t) = \lambda^2 \left[\frac{\sinh(\beta \hbar \omega_m)}{\cosh(\beta \hbar \omega_m) - \cos(\hbar \beta \kappa)} \cos(\omega_m t) \right. \\ \left. + \frac{\sin(\hbar \beta \kappa)}{\cosh(\beta \hbar \omega_m) - \cos(\hbar \beta \kappa)} \sin(\omega_m |t|) \right] e^{-\kappa |t|}, \quad (6)$$

$$L_2(t) = -\lambda^2 \frac{8\kappa\omega_m}{\hbar\beta} \sum_{n=1}^{\infty} \frac{v_n e^{-v_n |t|}}{(\Omega^2 + v_n^2)^2 - 4\kappa^2 v_n^2}$$

with the Matsubara frequencies $v_n = 2\pi n / (\hbar\beta)$ and

$$L''(t) = -\lambda^2 \sin(\omega_m t) e^{-\kappa |t|}. \quad (7)$$

In Lindblad description, a damped harmonic oscillator coupled to a thermal reservoir at inverse temperature β evolves according to

$$\dot{\rho} = -\frac{i}{\hbar} [H, \rho] + \mathcal{D}_{\kappa, \bar{n}} \rho \quad (8)$$

where here $H = \hbar \omega_m a^\dagger a$ is the Hamiltonian of the oscillator and its frequency ω_m already includes possible renormalizations due to the damping. The dissipator reads [44]

$$\mathcal{D}_{\kappa, \bar{n}} \rho = \kappa(\bar{n} + 1) [a\rho a^\dagger - a^\dagger a \rho] + \kappa \bar{n} [a^\dagger \rho a - a a^\dagger \rho] + \text{H.c.} \quad (9)$$

Using the quantum regression theorem we can obtain the reservoir correlation function $L_L(t) = L'_L(t) + iL''_L(t)$ for the damped harmonic oscillator in Lindblad description. We find that the real part

$$L'_L(t) = \lambda^2 \coth \left(\frac{\beta \hbar \omega_m}{2} \right) \cos(\omega_m t) e^{-\kappa |t|} \quad (10)$$

has a different functional form than $L'(t)$ in Eq. (6) while the imaginary part $L''_L(t)$ coincides with $L''(t)$ in Eq. (7) which is determined by $J_{\text{eff}}(\omega)$ of Eq. (5). Writing $L'_L(t)$ as in Eq. (4) we obtain $L'_L(t) = \frac{1}{\pi} \int_0^\infty d\omega \tilde{J}_{\text{eff}}(\omega) \coth(\beta\hbar\omega/2) \cos(\omega t)$ where

$$\tilde{J}_{\text{eff}}(\omega) = \lambda^2 \frac{\coth\left(\frac{\beta\hbar\omega_m}{2}\right)}{\coth\left(\frac{\beta\hbar\omega}{2}\right)} \left[\frac{\kappa}{\kappa^2 + (\omega - \omega_m)^2} + \frac{\kappa}{\kappa^2 + (\omega + \omega_m)^2} \right] \quad (11)$$

Despite the differences it is possible to obtain a very good agreement between the real parts $L'(t)$ and $L'_L(t)$ and their frequency space representations Eqs. (5) and (11). Ref. [45] estimates that the quantum regression theorem can only yield quantitatively correct predictions for the two-time correlation functions of the damped harmonic oscillator if $\kappa \ll \omega_m$ and $\hbar\beta\kappa \ll 1$. Indeed, under these assumptions we find very good agreement between $L'(t)$ and $L'_L(t)$. If we have good agreement between $L'(t)$ and $L'_L(t)$, we also find good agreement in frequency space. Note that while $\kappa \ll \omega_m$ is a necessary condition to derive the Lindblad equation (8) with the dissipator in Eq. (9), $\hbar\beta\kappa \ll 1$ puts a lower bound on the temperature where the identification of $L(t)$ and $L_L(t)$ is possible. On the other hand, also too high temperatures lead to deviations such that there is an intermediate temperature range where the best agreement is achieved (see [28] for a more detailed discussion).

In order to confirm the above considerations we simulated the dynamics of $\langle \sigma^z(t) \rangle$ for the full spin-boson Hamiltonian in Eq. (1) with spectral density $J_{\text{eff}}(\omega)$ from Eq. (5) using the numerically exact TEDOPA algorithm [6] and compared them with those given by Eq. (8) with $H = H_{\text{sb}}$ from Eq. (1) for a single mode. We considered an initial product state $|\uparrow\rangle\langle\uparrow| \otimes \rho_\beta$ and $\varepsilon = 0$, $\omega_m/2\pi = 100\text{kHz}$, $\kappa/2\pi = 1.25\text{kHz}$ as well as a spin-mode coupling $\lambda/2\pi = 100\text{kHz}$. We chose $\hbar\beta = 5.91 \cdot 10^{-6}\text{s}$ which corresponds to $\bar{n}(\omega_m) = 0.025$ for the Lindblad-damped oscillator and computed the evolution for spin energies $\Delta/2\pi = 50\text{kHz}$ and 100kHz . For both values of Δ we obtain very good agreement (see [28]) which shows that the analogy to the macroscopic environment also holds when we probe the spectral density away from the resonance. Note that one simulation for $\Delta/2\pi = 50\text{kHz}$ takes 15 days using 16 cores on a computing cluster which once more indicates the value of a trapped-ion simulator especially for structured environments and complex observables.

Trapped ion implementation. – Let us now proceed to illustrate how the ideas discussed above can be implemented in an ion-trap experiment. We consider N singly charged atomic ions with masses m_j confined in a linear Paul trap with effective harmonic trapping potential. We assume trapping conditions such that laser cooled ions form a linear Coulomb crystal along z with equilibrium positions $\mathbf{r}_j^0 = (0, 0, z_j^0)^T$. The motional degrees of freedom can then be described in terms of N uncoupled normal modes in each spatial direction [46, 47] and the motional Hamiltonian reads $H_m = \sum_{n,\alpha} \hbar\omega_{n,\alpha} a_{n,\alpha}^\dagger a_{n,\alpha}$ where $\omega_{n,\alpha}$ is the frequency of mode n in spatial direction $\alpha \in \{x, y, z\}$ with ladder operators $a_{n,\alpha}^\dagger, a_{n,\alpha}$.

For simplicity, we will focus on the case of a spin coupled

to a single damped mode which corresponds to a spin-boson model with Lorentzian spectral density as in Eq. (5). This system already exhibits an interesting phenomenology and has been studied with a variety of numerical and analytical approaches, see e.g. [48–51]. For this purpose we only need $N = 2$ ions: one ion is used to encode the spin while the other ion provides sympathetic cooling of the shared modes of motion. In order to avoid that the cooling lasers couple to the spin transition we choose to work with mixed species ion crystals. Alternatively, one could rely on single site addressing. The internal levels of the spin ion are described by the Hamiltonian $H_s = \hbar\frac{\omega_0}{2}\sigma^z$ while the internal levels of the coolant ion are adiabatically eliminated from the dynamics leading to the effective description in Eq. (9) of the cooling [41, 42].

For concreteness we consider a crystal composed of $^{24}\text{Mg}^+$ and $^{25}\text{Mg}^+$. $^{25}\text{Mg}^+$ has a nuclear spin and we can use the states $|F = 3, m_F = 3\rangle \equiv |\downarrow\rangle$ and $|F = 2, m_F = 2\rangle \equiv |\uparrow\rangle$ of the $^2S_{1/2}$ electronic hyperfine ground-state manifold to encode the spin. The spin can be driven by a microwave or in a two-photon stimulated Raman configuration while the desired coupling of the spin to the motional degrees of freedom in the σ^z basis is provided by a “walking standing wave”. In this configuration the spin states are off-resonantly coupled to the P manifold by two laser beams near 280nm whose beat note is tuned close to one of the motional mode frequencies [52]. The interaction of the ion with the applied fields is described by [28]

$$H_{\text{int}} = \hbar\frac{\Omega_d}{2}\sigma^+ e^{-i\omega_d t} + \hbar\frac{\Omega_{\text{odf}}}{2} e^{i(\mathbf{k}_L \mathbf{r} + \phi_L)} e^{-i\omega_L t} \sigma^z + \text{H.c.} \quad (12)$$

where Ω_d is the Rabi frequency of the applied microwave or stimulated Raman field and $\omega_d \approx \omega_0$ its frequency. Ω_{odf} , \mathbf{k}_L , ω_L , ϕ_L are the effective laser Rabi frequency, wave vector, frequency and phase, respectively. Directing \mathbf{k}_L along z the laser only couples to the motion along this axis. A two-ion crystal features two axial modes, an in- and an out-of-phase mode of motion with frequencies $\omega_{1,z} \equiv \omega_1$ and $\omega_{2,z} \equiv \omega_2$. The two modes are well separated in frequency such that choosing the laser frequency $\omega_L \approx \omega_2$ the spin only couples to the out-of-phase mode. In an interaction picture rotating with the microwave and motional frequencies and under the rotating wave approximation the system’s Hamiltonian reads [28]

$$H_{\text{sb1}} = \frac{\hbar\delta}{2}\sigma^z + \frac{\hbar\Omega_d}{2}\sigma^x - \frac{\hbar\lambda}{2}(a_2 + a_2^\dagger)\sigma^z + \hbar\delta_m a_2^\dagger a_2 \quad (13)$$

where $\delta = \omega_0 - \omega_d$ is the detuning of the field driving the spin transition and $\delta_m = \omega_2 - \omega_L \ll \omega_2$ the detuning of the laser from the motional mode. The spin-motion coupling is given by $\lambda = -i\eta_2 \Omega_{\text{odf}} e^{i(|\mathbf{k}_L|z_2^0 + \phi_L)}$ with the Lamb-Dicke factor $\eta_2 = \sqrt{\hbar/(2m_2\omega_2)} \tilde{M}_{22} |\mathbf{k}_L|$. Note that the laser phase can be chosen such that λ is real. \tilde{M}_{22} is the out-of-phase mode amplitude at the spin ion in mass weighted coordinates and m_2 its mass. Identifying $\hbar\delta = \varepsilon$, $\Omega_d = -\Delta$ and $\delta_m = \omega_m$ we obtain the spin-boson Hamiltonian of Eq. (1) for a single mode. Adding the cooling on the second ion the full system evolves according to Eq. (8) where $H = H_{\text{sb1}}$ from Eq. (13).

We simulate the dynamics of the system for experimentally realistic parameters. We consider an axial potential

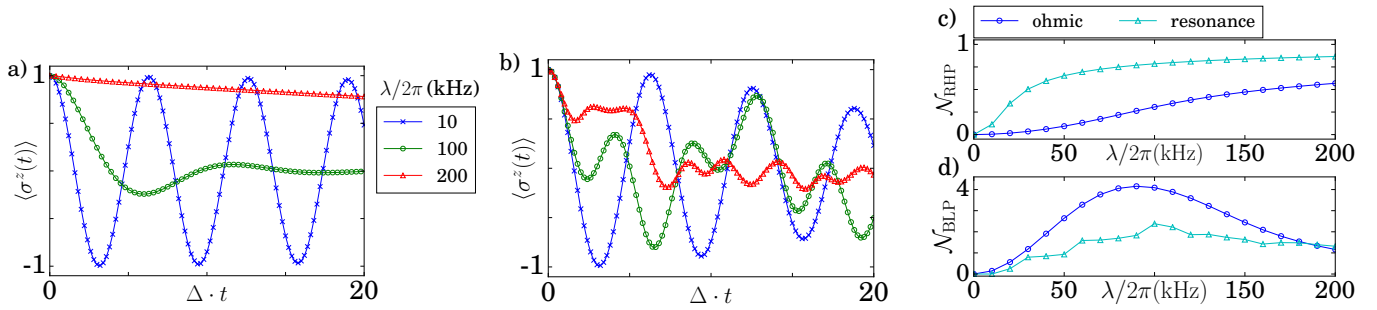


Figure 1: Parts **a)** and **b)** of the figure show the dynamics of $\langle \sigma_z(t) \rangle$ in natural time units $\Delta \cdot t$ under Eq. (8) with $H = H_{\text{sb1}}$ from Eq. (13), which corresponds to a spin-boson model with a Lorentzian spectral density as in Eq. (5), for varying spin-motion coupling λ . In part **a)** the spin energy $\Delta/2\pi = 3$ kHz is much smaller than the mode frequency $\omega_m/2\pi = 100$ kHz, so that the environment is approximately Ohmic. In part **b)** the mode is resonant with the spin ($\Delta/2\pi = 100$ kHz). The remaining parameters are given in the text. Part **c)** shows the measure of non-Markovianity \mathcal{N}_{RHP} in the intervals $[0, 0.01/\Delta]$ and $[0, 0.1/\Delta]$ for the ohmic and resonant cases, respectively. Part **d)** depicts the measure of non-Markovianity \mathcal{N}_{BLP} over the whole interval $[0, 20/\Delta]$ for both cases.

where a single $^{24}\text{Mg}^+$ ion has a center-of-mass frequency $\omega_{\text{com}}/2\pi = 2.54$ MHz which leads to an out-of-phase mode frequency $\omega_2/2\pi = 4.36$ MHz and $\eta_2 \approx 0.15$ for the mixed crystal where we assumed that the lasers inducing the spin-dependent force are at right angles. Furthermore, we assume that EIT cooling [42] is applied to the $^{24}\text{Mg}^+$ ion which has already been used to sympathetically cool mixed-species ion crystals [53]. We assume a cooling rate $2\kappa/2\pi = 2.5$ kHz and a steady-state population $\bar{n} = 0.025$ of the mode which is realistic in light of the results in [53]. Note that one has to make sure that the correspondence to the macroscopic environment holds for the effective mode frequency $\omega_m = \delta_m$ which is the detuning of the spin-motion coupling and thus much smaller than the physical mode frequency. We chose the field driving the spin to be resonant, i.e. $\varepsilon = 0$, and a detuning $\omega_m/2\pi = 100$ kHz of the spin-motion coupling such that we recover the parameters we used previously and the correspondence holds. In the simulations we truncate the motional Hilbert space at $n_{\text{max}} = 15$ excitations which makes truncation errors negligible.

In Fig. 1 we show the dynamics of $\langle \sigma_z(t) \rangle$ under Eq. (8) (where $H = H_{\text{sb1}}$ with the parameters from the previous paragraph) for an initial state $\rho_0 = |\uparrow\rangle\langle\uparrow| \otimes \rho_\beta$ where the thermal state ρ_β has a mean occupation number $\bar{n} = 0.025$. We vary the spin-motion coupling $\lambda/2\pi = 10 - 200$ kHz. In panel **a)** we show the dynamics for $\Delta/2\pi = 3$ kHz. In this case the spin samples the low frequencies of the spectral density in Eq. (5). Expanding the spectral density for small ω we obtain Ohmic behavior $J_{\text{eff}}(\omega) \sim \omega$. We observe a transition from damped to overdamped oscillations with increasing spin-mode coupling λ . This behavior is expected for an Ohmic spectral density at finite temperatures [3, 4]. Note, however, that our spectral density $J_{\text{eff}}(\omega)$, even if Ohmic for small frequencies, does not yield the same correlation function as a strict Ohmic environment. Therefore we can only expect qualitatively similar dynamics [48, 49]. In panel **b)** we show $\langle \sigma_z(t) \rangle$ for the same initial conditions and $\Delta/2\pi = 100$ kHz such that the spin is resonant with the mode. In this regime the spin dynamics shows a very complex behavior which one would intuitively

call non-Markovian.

Quantification of the degree of non-Markovianity of the dynamics.— In order to assess the non-Markovian character of the dynamics we compute two measures of non-Markovianity. The first measure, \mathcal{N}_{RHP} , arises from defining Markovianity in terms of the divisibility of the dynamical map of the dynamics [54], while the second, \mathcal{N}_{BLP} , is based on the definition that a dynamics is Markovian when yielding a monotonic decrease of state distinguishability [55]. We evaluated \mathcal{N}_{RHP} numerically [28] for the parameters of parts **a)** and **b)** of Fig. 1 over a time interval $[0, 0.01/\Delta]$ and $[0, 0.1/\Delta]$, respectively. The results are shown in part **c)** of the figure. In both cases the measure is non-zero for all couplings $\lambda/2\pi > 0$. An evaluation of \mathcal{N}_{RHP} requires process tomography and is therefore experimentally time-consuming already for a single spin. Hence, it might be easier to experimentally detect non-Markovian dynamics using \mathcal{N}_{BLP} which only requires state tomography. We numerically computed a lower bound on \mathcal{N}_{BLP} [28] for the parameters in parts **a)** and **b)** of Fig. 1 for the whole interval $[0, 20/\Delta]$. The results are shown in part **d)** of the figure. \mathcal{N}_{BLP} witnesses non-Markovianity in all regions where \mathcal{N}_{RHP} does, too. The somewhat discontinuous behavior of the curve for the resonant case is due to the finite time interval we are sampling.

In order to tailor more complex spectral densities than in this proof-of-principle experiment, one would need to couple the spin to two or more damped modes with the appropriate couplings and cooling rates that match the effective spectral density to the desired one. In case several modes are used it could be advantageous to use the transverse modes of motion. Due to the smaller bandwidth of the transverse phonon frequencies it is easier to couple to and cool several modes at the same time. It should be borne in mind that the cooling rates should be considerably smaller than the spacing between modes. Only then the damping of each mode can be described by a dissipator as in Eq. (9). In order to fill possibly unwanted gaps in the effective spectral density one could then use the modes of the second transverse direction of motion and place the effective frequencies of these modes between those of the

first direction.

Let us finally note that the model can be extended not only to more complex spectral densities by including more ions and thus modes but also to include more spins. Then trapped ions could be used as a testbed for the dynamics of exciton transport in complex spectral densities and especially the determination of higher order spectral responses, e.g. 2D electronic spectroscopy, which are exceedingly hard to compute numerically even for only a few electronic sites and a structured spectral density [11].

In summary, we have shown that spin-boson models with continuous spectral densities can be simulated using damped oscillators in Lindblad description. This leads to a significant reduction of the technical requirements for the implementa-

tion of this paradigmatic model for decoherence and dissipation employing trapped ions. The joint effect of different damped modes allows one to tailor a variety of spectral densities with rich non-Markovian features. We showed that it is possible to carry out simulations of non-trivial dynamics making use of just one motional mode, and illustrated the practicality of our approach by simulating an experiment with realistic parameters.

Acknowledgements.— A. L. and D. T. acknowledge very useful discussions with A. Smirne. This work was supported by an Alexander-von-Humboldt Professorship, the ERC synergy grant BioQ and EU projects EQUAM and QUCHIP. Computational resources were provided by the bwUniCluster and the bwForCluster JUSTUS.

-
- [1] A. Garg, J. N. Onuchic, and V. Ambegaokar, *Effect of friction on electron transfer in biomolecules*. J. Chem. Phys. **83**, 4491 (1985).
- [2] X. Dong and K. Schulten, *Coupling of protein motion to electron transfer in a photosynthetic reaction center: investigating the low temperature behavior in the framework of the spin-boson model*. Chem. Phys. **182**, 91 (1994).
- [3] U. Weiss, *Quantum Dissipative Systems* (World Scientific, Singapore, 2007), Third Edition.
- [4] A.J. Leggett, S. Chakravarty, A. T. Dorsey, M. P. A. Fisher, A. Garg and, W. Zwerger, *Dynamics of the Dissipative Two State System*. Rev. Mod. Phys. **59**, 1 (1987).
- [5] R. Bulla, T. A. Costi, and T. Pruschke, *Numerical renormalization group method for quantum impurity systems*. Rev. Mod. Phys. **70**, 395 (2008).
- [6] A. Chin, A. Rivas, S. F. Huelga, and M. B. Plenio, *Exact mapping between system-reservoir quantum models and semi-infinite discrete chains using orthogonal polynomials*. J. Math. Phys. **51**, 092109 (2010).
- [7] J. Prior, A. W. Chin, S. F. Huelga, and M. B. Plenio, *Efficient Simulation of Strong System-Environment Interactions*. Phys. Rev. Lett. **105**, 050404 (2010).
- [8] R. Egger and C. H. Mak, *Low-temperature dynamical simulation of spin-boson systems*. Phys. Rev. B **50**, 15210 (1994).
- [9] N. Makri, *Numerical path integral techniques for long time dynamics of quantum dissipative systems*. J. Math. Phys. **36**, 2430 (1995).
- [10] S. F. Huelga and M. B. Plenio, *Vibrations, Quanta and Biology*. Contemp. Phys. **54**, 181 (2013).
- [11] M. B. Plenio, J. Almeida, and S. F. Huelga, *Origin of long-lived oscillations in 2D-spectra of a quantum vibronic model: Electronic versus vibrational coherence*, J. Chem. Phys. **139**, 235102 (2013).
- [12] M. Mielenz, J. Brox, S. Kahra, G. Leschhorn, M. Albert, T. Schaetz, H. Landa, and B. Reznik, *Trapping of Topological-Structural Defects in Coulomb Crystals* Phys. Rev. Lett. **110**, 133004 (2013).
- [13] S. Ulm, J. Roßnagel, G., Jacob, C., Degntner, S. T. Dawkins, U.G. Poschinger, R. Nigmatullin, A. Retzker, M. B. Plenio, F. Schmidt-Kaler, and K. Singer, *Observation of the Kibble-Zurek scaling law for defect formation in ion crystals*. Nature Comm. **4**, 2290 (2013).
- [14] K. Pyka, J. Keller, H. L. Partner, R. Nigmatullin, T. Burgermeister, D. M. Meier, K. Kuhlmann, A. Retzker, M. B. Plenio, W. H. Zurek, and A. Del Campo, *Topological defect formation and spontaneous symmetry breaking in ion Coulomb crystals*. Nature Comm. **4**, 2291 (2013).
- [15] See R. Blatt and C. F. Roos, *Quantum simulations with trapped ions*. Nat. Phys. **8**, 277 (2012), and references therein.
- [16] Ch. Schneider, D. Porras, and T. Schaetz, *Experimental quantum simulations of many-body physics with trapped ions* Rep. Prog. Phys. **75**, 024401 (2012).
- [17] J. T. Barreiro, M. Müller, P. Schindler, D. Nigg, T. Monz, M. Chwalla, M. Hennrich, C. F. Roos, P. Zoller, and R. Blatt, *An open-system quantum simulator with trapped ions*, Nature **470**, 486 (2011)
- [18] M. Gessner, M. Ramm, T. Pruttivarasin, A. Buchleitner, H-P. Breuer and H. Häffner, *Local detection of quantum correlations with a single trapped ion*, Nat. Phys. **10**, 105 (2014)
- [19] J. Smith, A. Lee, P. Richerme, B. Neyenhuis, P. W. Hess, P. Hauke, M. Heyl, D. A. Huse, and C. Monroe, *Many-body localization in a quantum simulator with programmable random disorder*, Nat. Phys. **12**, 907 (2016)
- [20] G. Clos, D. Porras, U. Warring, and T. Schaetz, *Time-resolved observation of thermalization in an isolated quantum system.*, Phys. Rev. Lett. **117**, 170401 (2016).
- [21] D. Porras, F. Marquardt, J. von Delft, and J. I. Cirac, *Mesoscopic spin-boson models of trapped ions*. Phys. Rev. A **78**, 010101(R) (2008).
- [22] A. Imamoglu, *Stochastic wave-function approach to non-Markovian systems*. Phys. Rev. A **50**, 3650 (1994).
- [23] P. Stenius, and A. Imamoglu, *Stochastic wavefunction methods beyond the Born - Markov and rotating-wave approximations*. Quantum Semiclass. Opt. **8**, 283 (1996).
- [24] B. M. Garraway, *Nonperturbative decay of an atomic system in a cavity*. Phys. Rev. A **55**, 2290 (1997).
- [25] B. J. Dalton, S. M. Barnett, and B. M. Garraway, *Theory of pseudomodes in quantum optical processes*. Phys. Rev. A **64**, 053813 (2001).
- [26] R. P. Feynman, A. R. Hibbs, and D. F. Styer, *Quantum mechanics and path integrals* (Emended Edition, Dover Publications, Mineola, 2010).
- [27] R. P. Feynman, and F. L. Vernon, *The Theory of a General Quantum System Interacting with a Linear Dissipative System*. Ann. Phys. (N.Y.) **24**, 118 (1963).
- [28] See the Supplemental Material which includes references [29] through [39] for details and derivations.
- [29] M. P. Woods, M. Cramer, and M. B. Plenio, *Simulating Bosonic*

- Baths with Error Bars*. Phys. Rev. Lett. **115**, 130401 (2015).
- [30] G. Vidal, *Efficient Simulation of One-Dimensional Quantum Many-Body Systems*. Phys. Rev. Lett. **93**, 040502 (2004).
- [31] U. Schollwöck, *The density-matrix renormalization group in the age of matrix product states*. Ann. Phys. **326**, 96 (2011).
- [32] W. Gautschi, *Algorithm 726: ORTHPOL—A Package of Routines for Generating Orthogonal Polynomials and Gauss-type Quadrature Rules*. ACM Trans. Math. Softw. **20**, 21 (1994).
- [33] D. Tamascelli, R. Rosenbach, and M. B. Plenio, *Improved scaling of time-evolving block-decimation algorithm through reduced-rank randomized singular value decomposition*, Phys. Rev. E. **91**, 063306 (2015).
- [34] F. Reiter and A. S. Sørensen, *Effective operator formalism for open quantum systems*. Phys. Rev. A **85**, 032111 (2012).
- [35] D. J. Wineland, M. Barrett, J. Britton, J. Chiaverini, B. DeMarco, W. M. Itano, B. Jelenković, C. Langer, D. Leibfried, V. Meyer, T. Rosenband, and T. Schaetz, *Quantum information processing with trapped ions.*, Phil. Trans. R. Soc. Lond. A **361**, 1349 (2003)
- [36] A. Sørensen, and K. Mølmer, *Quantum Computation with Ions in Thermal Motion*. Phys. Rev. Lett. **82**, 1971 (1999).
- [37] K. Zyczkowski, and I. Bengtsson *On duality between quantum maps and quantum states*, (arXiv:quant-ph/0401119) Open Syst. Inf. Dyn. **11**, 3-42 (2004)
- [38] S. Wißmann, A. Karlsson, E.-M. Laine, J. Piilo, and H.-P. Breuer, *Optimal state pairs for non-Markovian quantum dynamics*. Phys. Rev. A **86**, 062108 (2012)
- [39] M. Wittemer, G. Clos, H.-P. Breuer, U. Warring, and T. Schaetz, *Probing Quantum Memory Effects with High Resolution*, arXiv:1702.07518
- [40] C. Meier and D. J. Tannor, *Non-Markovian evolution of the density operator in the presence of strong laser fields*. J. Chem. Phys. **111**, 3365 (1999).
- [41] J. I. Cirac, R. Blatt, P. Zoller, and W. D. Phillips, *Laser cooling of trapped ions in a standing wave*. Phys. Rev. A **46**, 2668 (1992).
- [42] G. Morigi, *Cooling atomic motion with quantum interference*. Phys. Rev. A **67**, 033402 (2003).
- [43] H. Grabert, U. Weiss, and P. Talkner, *Quantum Theory of the Damped Harmonic Oscillator*. Z. Phys. B - Condensed Matter **55**, 87 (1984).
- [44] H.-P. Breuer and F. Petruccione, *The Theory of Open Quantum Systems* (Oxford University Press, Oxford, 2002).
- [45] P. Talkner, *The failure of the Quantum Regression Hypothesis*. Ann. Phys. **167**, 390 (1986).
- [46] D. F. V. James, *Quantum dynamics of cold trapped ions with application to quantum computation* Appl. Phys. B **66**, 181 (1998)
- [47] G. Morigi and H. Walther, *Two-species Coulomb chains for quantum information*. Eur. Phys. J. D **13**, 261 (2001).
- [48] F. K. Wilhelm, S. Kleff, and J. von Delft, *The spin-boson model with a structured environment: a comparison of approaches*. Chem. Phys. **296**, 345 (2004).
- [49] M. Thorwart, E. Paladino, and M. Grifoni, *Dynamics of the spin-boson model with a structured environment*. Chem. Phys. **296**, 333 (2004).
- [50] J. C. Escher, and J. Ankerhold, *Quantum dynamics of a two-level system in a structured environment: Numerical study beyond perturbation theory*. Phys. Rev. A **83**, 032122 (2011).
- [51] F. Brito and A. O. Caldeira, *Dissipative dynamics of a two-level system resonantly coupled to a harmonic mode*. New J. Phys. **10**, 115014 (2008).
- [52] A. Friedenauer, H. Schmitz, J. T. Glueckert, D. Porras, and T. Schaetz, *Simulating a quantum magnet with trapped ions*. Nat. Phys. **4**, 757 (2008).
- [53] Y. Lin, J. P. Gaebler, T. R. Tan, R. Bowler, J.D. Jost, D. Leibfried, and D. J. Wineland, *Sympathetic Electromagnetically-Induced-Transparency Laser Cooling of Motional Modes in an Ion Chain*. Phys. Rev. Lett. **110**, 153002 (2013).
- [54] A. Rivas, S. F. Huelga, M. B. Plenio, *Quantum non-Markovianity: characterization, quantification and detection*. Rep. Prog. Phys. **77**, 094001 (2014).
- [55] H.-P. Breuer, E.-M. Laine, J. Piilo, and B. Vacchini, *Colloquium: Non-Markovian dynamics in open quantum systems*. Rev. Mod. Phys. **88**, 021002 (2016).

I. SUPPLEMENTAL MATERIAL TO “SIMULATING SPIN-BOSON MODELS WITH TRAPPED IONS”

Contents

References	5
I. Supplemental Material to “Simulating spin-boson models with trapped ions”	7
A. Effective spectral densities of damped harmonic oscillators	7
1. Time domain considerations	7
2. Frequency space considerations	10
B. tDMRG simulations using the TEDOPA algorithm	11
C. Spin-dependent optical dipole forces	12
D. Spin-boson Hamiltonian with trapped ions	14
E. Computation of non-Markovianity measures	15
References	16

Appendix A: Effective spectral densities of damped harmonic oscillators

We start by briefly surveying the quantities that we need for the discussion of the effective spectral densities of damped harmonic oscillators. We consider the spin-boson model where a spin is coupled to a bath of harmonic oscillators. The spin constitutes the principal system and the bath consists of an infinite set of independent harmonic oscillators. This is an archetypical model for a two-state system coupled to a dissipative environment and is conveniently modeled by the Hamiltonian [1]

$$H_{\text{sb}} = \frac{\varepsilon}{2}\sigma^z - \frac{\hbar\Delta}{2}\sigma^x + \frac{1}{2}\sum_n \left[\frac{p_n^2}{m_n} + m_n\omega_n^2 x_n^2 - c_n q_0 \sigma^z x_n \right] \quad (\text{A1})$$

where $\sigma^z = |\uparrow\rangle\langle\uparrow| - |\downarrow\rangle\langle\downarrow|$ and $\sigma^x = |\uparrow\rangle\langle\downarrow| + |\downarrow\rangle\langle\uparrow|$ denote the usual Pauli matrices, ε the energy splitting of the spin states and $\hbar\Delta$ their coupling. p_n and x_n denote the canonical momenta and coordinates of the environmental modes of frequency ω_n , q_0 is some characteristic length scale and c_n describes the coupling of mode n to the spin. Quantizing the environmental oscillators $x_n = \sqrt{\hbar/(2m_n\omega_n)}(a_n + a_n^\dagger)$ so that a_n and a_n^\dagger denote the ladder operators of oscillator n we can write the spin-mode coupling as

$$\hbar\lambda_n = c_n q_0 \sqrt{\hbar/(2m_n\omega_n)}. \quad (\text{A2})$$

The spin-boson Hamiltonian can then be written as

$$H_{\text{sb}} = \frac{\varepsilon}{2}\sigma^z - \frac{\hbar\Delta}{2}\sigma^x - \frac{1}{2}\sigma^z \sum_n \hbar\lambda_n (a_n^\dagger + a_n) + \sum_n \hbar\omega_n a_n^\dagger a_n \quad (\text{A3})$$

which is Eq. (1) of the main text. Note that we have omitted the ground-state energies of the oscillators. For an initial product state of spin and environment where the environment is in a thermal state at inverse temperature β the influence of the oscillator environment on the spin is given by the influence functional $F[q, q']$ in Eq. (3) of the main text which is in turn determined by the reservoir correlation function [1]

$$L(t) = \frac{1}{\hbar^2} \langle X(t)X(0) \rangle_\beta \quad (\text{A4})$$

with the collective coordinate $X(t) = q_0 \sum_n c_n x_n = \sum_n \hbar\lambda_n (a_n + a_n^\dagger)$. The reservoir correlation function can be equivalently given in terms of the spectral density $J(\omega)$

$$L(t) = \frac{1}{\pi} \int_0^\infty d\omega J(\omega) \left[\coth\left(\frac{\beta\hbar\omega}{2}\right) \cos(\omega t) - i \sin(\omega t) \right]. \quad (\text{A5})$$

It is known that an oscillator damped by a bath with Ohmic spectral density produces an effective environment with Lorentzian spectral density [2]. Here, we inspect in more detail when the same can be done for the damped harmonic oscillator in Lindblad description. To this end, it is instructive to start from the time domain and consider $L(t)$ for the two cases.

1. Time domain considerations

The reservoir correlation function $L(t)$ in Eq. (A4) may be written explicitly in terms of the environmental coordinate correlation functions using $X(t) = q_0 \sum_n c_n x_n$

$$L(t) = q_0^2 \sum_n \frac{c_n^2}{\hbar^2} \langle x_n(t)x_n(0) \rangle_\beta \quad (\text{A6})$$

where we have used that the oscillators are independent. In the following we consider only a single oscillator and therefore omit the index n from now on. The function $\langle x(t)x(0) \rangle_\beta$ is in general a complex function and we can write it in terms of its real and imaginary parts

$$\langle x(t)x(0) \rangle_\beta = S(t) + iA(t) \quad (\text{A7})$$

where

$$S(t) = \frac{1}{2} \langle \{x(t), x(0)\} \rangle_\beta, \quad (\text{A8})$$

$$A(t) = \frac{1}{2i} \langle [x(t), x(0)] \rangle_\beta. \quad (\text{A9})$$

The imaginary part $A(t)$ is related to the damped oscillator's response function $\chi(t)$ through $\chi(t) = -\frac{2}{\hbar}\Theta(t)A(t)$ [1] where $\Theta(t)$ is the Heaviside step function. Note that accordingly also $L(t)$ is a complex function

$$L(t) = L'(t) + iL''(t). \quad (\text{A10})$$

Let us now consider a damped oscillator that evolves according to the Lindblad equation given in Eq. (8) of the main text

$$\dot{\rho} = -i[\omega_m a^\dagger a, \rho] + \mathcal{D}_{\kappa, \bar{n}} \rho \quad (\text{A11})$$

with dissipator

$$\begin{aligned} \mathcal{D}_{\kappa, \bar{n}} \rho = & \kappa(\bar{n} + 1)[a\rho a^\dagger - a^\dagger a\rho] \\ & + \kappa\bar{n}[a^\dagger \rho a - a a^\dagger \rho] + \text{H.c.} \end{aligned} \quad (\text{A12})$$

given in Eq. (9) of the main text. The above dissipator takes the mode populations to a thermal state with mean occupation number \bar{n} at a rate 2κ . We can compute the coordinate correlation function $\langle x(t)x(0) \rangle_{\beta, L} = S_L(t) + iA_L(t)$ of the damped harmonic oscillator in Lindblad description using the quantum regression theorem:

$$S_L(t) = \frac{\hbar}{2m\omega_m} \coth\left(\frac{\beta\hbar\omega_m}{2}\right) \cos(\omega_m t) e^{-\kappa|t|} \quad (\text{A13})$$

and

$$A_L(t) = -\frac{\hbar}{2m\omega_m} \sin(\omega_m t) e^{-\kappa|t|}. \quad (\text{A14})$$

Here m is the mass of the oscillator. Note that the frequency ω_m is taken to include possible renormalizations of the mode frequency due to the damping and $\kappa \ll \omega_m$ is necessary to derive the Lindblad equation above. Inserting the result into Eq. (A6) and using Eq. (A2) we obtain the real and imaginary parts $L'_L(t)$ and $L''_L(t)$ of $L_L(t)$ from Eqs. (10) and (7) of the main text

$$L'_L(t) = \lambda^2 \coth\left(\frac{\beta\hbar\omega_m}{2}\right) \cos(\omega_m t) e^{-\kappa|t|} \quad (\text{A15})$$

and

$$L''_L(t) = -\lambda^2 \sin(\omega_m t) e^{-\kappa|t|}. \quad (\text{A16})$$

As we stated earlier we have $\chi(t) = -\frac{2}{\hbar}\Theta(t)A(t)$. Inserting $A_L(t)$ into the previous equation yields the response function of the classical damped harmonic oscillator. Having in mind that an Ohmic spectral density leads to the classical equation of motion for a damped oscillator [1], and thus the same response function, it seems appropriate to compare the regression theorem results to that of the oscillator damped by an Ohmic bath.

Therefore, we move on to the harmonic oscillator damped by a thermal oscillator bath with Ohmic spectral density. For this case, it is also possible to calculate the coordinate correlation function $\langle x(t)x(0) \rangle_\beta$ analytically [1, 3]. We denote the free oscillation frequency of the oscillator by Ω while we denote the damping rate on the oscillator's coordinate by κ_{ohm} . In the underdamped regime $\kappa_{\text{ohm}} < \Omega$ the oscillator's frequency is reduced to $\omega_r = \sqrt{\Omega^2 - \kappa_{\text{ohm}}^2}$ due to the damping. Since we want to compare the results to the Lindblad case where $\kappa \ll \omega_m$ we will always have $\kappa_{\text{ohm}} \ll \Omega$ such that we are in the underdamped regime. In this regime the real part of the coordinate correlation $S(t)$ splits in two parts [1]

$$S(t) = S_1(t) + S_2(t) \quad (\text{A17})$$

with

$$\begin{aligned} S_1(t) = & \frac{\hbar}{2m\omega_r} \left[\frac{\sinh(\beta\hbar\omega_r)}{\cosh(\beta\hbar\omega_r) - \cos(\beta\hbar\kappa_{\text{ohm}})} \cos(\omega_r t) \right. \\ & \left. + \frac{\sin(\beta\hbar\kappa_{\text{ohm}})}{\cosh(\beta\hbar\omega_r) - \cos(\beta\hbar\kappa_{\text{ohm}})} \sin(\omega_r |t|) \right] e^{-\kappa_{\text{ohm}}|t|} \end{aligned} \quad (\text{A18})$$

and

$$S_2(t) = -\frac{4\kappa_{\text{ohm}}}{m\beta} \sum_{n=1}^{\infty} \frac{v_n e^{-v_n|t|}}{(\Omega^2 + v_n^2)^2 - 4\kappa_{\text{ohm}}^2 v_n^2} \quad (\text{A19})$$

where the $v_n = 2\pi n/(\hbar\beta)$ are the Matsubara frequencies. The imaginary part reads

$$A(t) = -\frac{\hbar}{2m\omega_r} \sin(\omega_r t) e^{-\kappa_{\text{ohm}}|t|}. \quad (\text{A20})$$

Comparing Eqs. (A20) and (A14) we see that the imaginary parts $A(t)$ and $A_L(t)$ are exactly equal for $\omega_r = \omega_m$ and $\kappa_{\text{ohm}} = \kappa$ which we will assume from now on. With this substitution and inserting Eqs. (A18)-(A20) into Eq. (A6) we obtain $L(t) = L'(t) + iL''(t) = L_1(t) + L_2(t) + iL''(t)$ where

$$\begin{aligned} L_1(t) = & \lambda^2 \left[\frac{\sinh(\beta\hbar\omega_m)}{\cosh(\beta\hbar\omega_m) - \cos(\beta\hbar\kappa)} \cos(\omega_m t) \right. \\ & \left. + \frac{\sin(\beta\hbar\kappa)}{\cosh(\beta\hbar\omega_m) - \cos(\beta\hbar\kappa)} \sin(\omega_m |t|) \right] e^{-\kappa|t|}, \end{aligned} \quad (\text{A21})$$

$$L_2(t) = -\lambda^2 \frac{8\kappa\omega_m}{\hbar\beta} \sum_{n=1}^{\infty} \frac{v_n e^{-v_n|t|}}{(\Omega^2 + v_n^2)^2 - 4\kappa^2 v_n^2}$$

and

$$L''(t) = -\lambda^2 \sin(\omega_m t) e^{-\kappa|t|} \quad (\text{A22})$$

recovering Eqs. (6) and Eq. (7) of the main text.

The symmetric parts $S(t)$ and $S_L(t)$ do not coincide after the substitution $\omega_r = \omega_m$ and $\kappa_{\text{ohm}} = \kappa$. Hence, in the following we seek the regimes where the two functions coincide. In order to identify $S_L(t)$ with $S(t)$ we need to be able to neglect $S_2(t)$ as well as the sine component in $S_1(t)$. We start by considering $S_2(t)$. The argument follows Refs. [3, 4]. The Matsubara frequencies v_n determine the time scale on which $S_2(t)$ decays, the smallest decay rate being v_1 . Accordingly, if the decay rate κ is much smaller than the smallest Matsubara frequency, $S_2(t)$ drops to zero much faster than $S_1(t)$. This is the regime where

$$\frac{\kappa\hbar\beta}{2\pi} = \frac{\kappa}{v_1} \ll 1. \quad (\text{A23})$$

In this regime one expects that $S_2(t)$ will only produce deviations on very short time scales and is negligible if we are interested in not too short time scales. This is the case in our considerations. If $S_2(0) \ll S_1(0)$ we can neglect $S_2(t)$ completely.

Assuming we can disregard $S_2(t)$ we need to find the regime where

$$S_L(t) \approx S_1(t). \quad (\text{A24})$$

In the limit $\beta\hbar\kappa \ll 1$ we can expand the sine and cosine terms in $S_1(t)$ in this small parameter and to first order we obtain

$$\begin{aligned} S_1(t) &\approx \frac{\hbar}{2m\omega_m} \left[\frac{\sinh(\beta\hbar\omega_m)}{\cosh(\beta\hbar\omega_m) - 1} \cos(\omega_m t) \right. \\ &\quad \left. + \frac{\hbar\beta\kappa}{\cosh(\beta\hbar\omega_m) - 1} \sin(\omega_m |t|) \right] e^{-\kappa|t|} \quad (\text{A25}) \\ &\approx \frac{\hbar}{2m\omega_m} \frac{\sinh(\beta\hbar\omega_m)}{\cosh(\beta\hbar\omega_m) - 1} \cos(\omega_m t) e^{-\kappa|t|} \end{aligned}$$

where we have used $\hbar\beta\kappa \ll \sinh(\hbar\beta\omega_m)$ in the last step. Using the identity $\coth \frac{x}{2} = \sinh(x)/(\cosh x - 1)$ finally yields $S_1(t) = S_L(t)$ if the reservoirs are at the same inverse temperature β . Accordingly, we assume that the reservoir in the Lindblad description and the Ohmic oscillator bath have the same inverse temperature β from now on.

Thus, we have established a regime where the coordinate correlation function of the Lindblad damped harmonic oscillator approximately coincides with that of an oscillator damped by a reservoir with Ohmic spectral density. In this regime the Lindblad damped oscillator should act as a macroscopic reservoir with Lorentzian spectral density as in Eq. (5) of the main text.

Note that for a given cooling rate κ the condition in Eq. (A23) puts a lower bound on the temperature where we can neglect $S_2(t)$ and thus a lower bound on the temperature where the Lindblad damped oscillator produces the same coordinate correlation function as the oscillator damped by a reservoir with Ohmic spectral density. Thus, we require $\kappa \ll \omega_m$ and $\frac{\kappa\hbar\beta}{2\pi} \ll 1$ to make the identification. Indeed, Refs. [3, 4] estimate that the quantum regression theorem can only yield quantitatively correct predictions for the two-time correlation functions of the damped harmonic oscillator if the two above conditions are met.

For ion-trap experiments one usually considers the mean occupation number \bar{n} of the bosonic modes rather than their temperature and therefore it is desirable to cast condition (A23) in a form where it depends on \bar{n} . Assuming a thermal state for a bosonic mode we can associate the temperature $T_{\text{eff}} = \hbar\omega/[k_B \log(1 + 1/\bar{n})]$ to the mode and the condition in Eq. (A23) becomes

$$\frac{\log(1 + \frac{1}{\bar{n}})}{2\pi} \frac{\kappa}{\omega_m} \ll 1. \quad (\text{A26})$$

Note that in the ion-trap implementation the mode frequency is an effective frequency much smaller than the physical frequency of the mode (see App. D). Therefore, one has to make sure the above condition is met for the effective frequency such that the correspondence to the effective harmonic environment is not lost.

In order to make the above considerations more quantitative and illustrate that the match of the reservoir correlation functions is indeed very good we make a numerical comparison of the functions $L(t)$ and $L_L(t)$ in the regime $\kappa \ll \omega_m, v_1$. Since the imaginary parts of the two functions are equal we focus on the real parts $L'(t)$ and $L'_L(t)$. In Fig. 2 we plot $L'(t)/\lambda^2$ including the first 10^4 Matsubara frequencies together with $L_L(t)$ for $\omega_m/2\pi = 100$ kHz, $\kappa/2\pi = 1.25$ kHz

and a mean occupation number $\bar{n}(\omega_m) = 0.025$ which corresponds to $\hbar\beta = 5.91 \cdot 10^{-6}$ s. These parameters are realistic in an ion trap experiment. In part **a)** of the figure we compare $L'(t)$ and $L'_L(t)$ on short and in part **b)** on intermediate time scales. One can appreciate excellent agreement between the two functions.

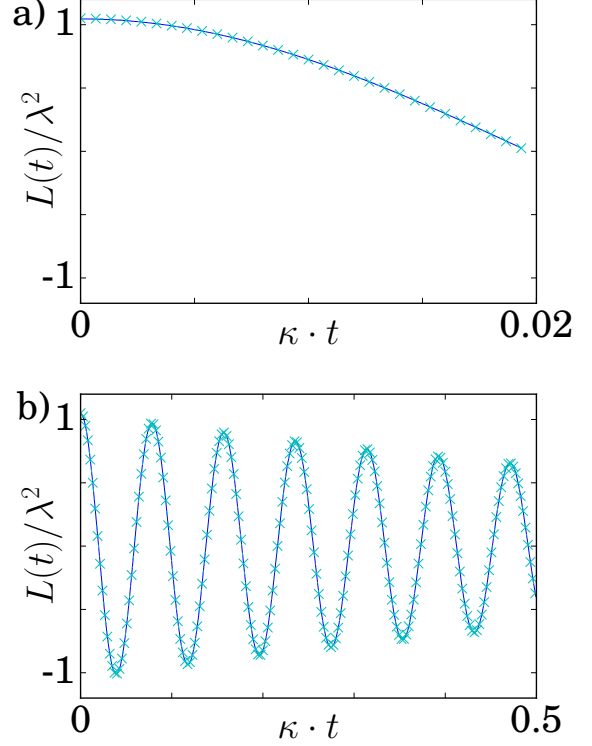


Figure 2: Comparison of $L'(t) = L_1(t) + L_2(t)$ from Eq. (A21) including the first 10^4 Matsubara frequencies (blue solid lines) and $L'_L(t)$ from Eq. (A15) (dashed-dot line and crosses) for $\omega_m/2\pi = 100$ kHz, $\kappa/2\pi = 1.25$ kHz and $\bar{n}(\omega_m) = 0.025$ ($\hbar\beta = 5.91 \cdot 10^{-6}$ s). Panel **a)** shows the time evolution for short times, while panel **b)** illustrates the intermediate time behavior.

In order to illustrate for which parameters the approximation works well we compute the distance

$$d = \frac{1}{\lambda^2} \left| \int_0^\infty dt [L(t) - L_L(t)] \right| \quad (\text{A27})$$

between the functions $L(t)$ and $L_L(t)$ which can be evaluated analytically to yield

$$\begin{aligned} d &= c_q \frac{\kappa}{\kappa^2 + \omega_m^2} + c_{cl} \frac{\omega_m}{\kappa^2 + \omega_m^2} \\ &\quad - \frac{8\kappa\omega_m}{\hbar\beta} \sum_{n=1}^{\infty} \frac{1}{(\omega_m^2 + \kappa^2 + v_n^2)^2 - 4\kappa^2 v_n^2}, \end{aligned} \quad (\text{A28})$$

where we used the abbreviations

$$\begin{aligned} c_q &= \frac{\sinh(\beta\hbar\omega_m)}{\cosh(\beta\hbar\omega_m) - \cos(\hbar\beta\kappa)} - \coth\left(\frac{\hbar\beta\omega_m}{2}\right), \\ c_{cl} &= \frac{\sin(\beta\hbar\kappa)}{\cosh(\beta\hbar\omega_m) - \cos(\hbar\beta\kappa)}. \end{aligned}$$

We evaluate the difference for different cooling rates and mean occupation numbers while keeping the mode frequency fixed at $\omega_m/2\pi = 100\text{kHz}$. The results are depicted in Fig. 3. Note that higher bars in the figure correspond to smaller values of d . We observe that increasing κ increases the difference between the two functions. For a fixed cooling rate we observe that the distance is minimal for intermediate values of \bar{n} . This can be understood by considering Eqs. (A15) and (A21). In order to identify $L(t)$ and $L_L(t)$ we need to be able to neglect $L_2(t)$ and the sine component in $L_1(t)$. The condition in Eq. (A23) provides the regime where $L_2(t)$ is negligible and favors higher temperatures. However, in order to suppress the sine component in $L_1(t)$ lower temperatures are more favorable. Thus, we obtain the best match for intermediate temperatures.

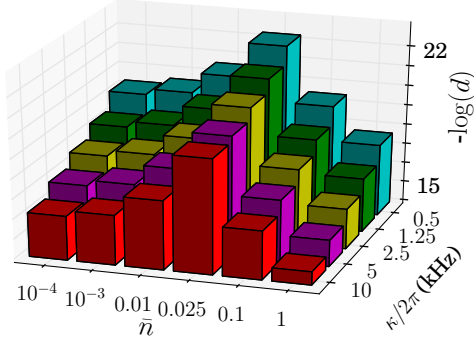


Figure 3: The figure shows the distance d , Eq. (A27), between the correlation functions $L(t)$ including the first 10^4 Matsubara frequencies and $L_L(t)$ for different values of the cooling rate κ and mean occupation number \bar{n} for fixed mode frequency $\omega_m/2\pi = 100\text{kHz}$. Higher bars correspond to smaller values of d .

2. Frequency space considerations

In [2] Garg *et al.* show that a harmonic oscillator which in turn is damped by an oscillator environment with Ohmic spectral density with infinite cutoff produces the effective spectral density

$$\frac{q_0^2}{\hbar} J_{\text{eff,ohm}}(\omega) = \frac{q_0^2 c_1^2}{\hbar m} \frac{2\kappa\omega}{(\Omega^2 - \omega^2)^2 + 4\omega^2\kappa^2}. \quad (\text{A29})$$

Here, κ is the damping induced by the bath on the coordinate of the oscillator, Ω and m its free oscillation frequency and mass, respectively, and $q_0 c_1$ its coupling to the spin [see Eq. (A1)]. Note that upon writing the influence functional as in Eq. (3) of the main text we have absorbed the prefactor q_0^2/\hbar into the spectral density. Using Eq. (A2) and setting $\omega_m^2 = \Omega^2 - \kappa^2$ one obtains the spectral density $J_{\text{eff}}(\omega)$ in Eq. (5) of the main text

$$J_{\text{eff}}(\omega) = \lambda^2 \left[\frac{\kappa}{\kappa^2 + (\omega - \omega_m)^2} - \frac{\kappa}{\kappa^2 + (\omega + \omega_m)^2} \right]. \quad (\text{A30})$$

In the previous section we have seen that in a certain parameter regime the Lindblad description of the damped harmonic oscillator reproduces the coordinate correlation function and thus $L(t)$ of the oscillator damped by an Ohmic bath. $L(t)$ can also be written in terms of the spectral density $J(\omega)$ according to Eq. (A5). In fact, in almost all cases environments are characterized by their spectral density rather than their correlation functions. Therefore, we analyze the effective spectral density of the Lindblad-damped oscillator and compare it to the Lorentzian spectral density $J_{\text{eff}}(\omega)$ in Eq. (A30) above.

The Fourier representation of $L_L(t)$ in Eqs. (A15) and (A16) reads

$$L_L(t) = \frac{1}{\pi} \int_0^\infty d\omega \left[\tilde{J}_{\text{eff}}(\omega) \coth\left(\frac{\hbar\beta\omega}{2}\right) \cos(\omega t) - i J_{\text{eff}}(\omega) \sin(\omega t) \right] \quad (\text{A31})$$

with $J_{\text{eff}}(\omega)$ as in Eq. (A30) above and

$$\tilde{J}_{\text{eff}}(\omega) = \lambda^2 \frac{\coth\left(\frac{\beta\hbar\omega_m}{2}\right)}{\coth\left(\frac{\beta\hbar\omega}{2}\right)} \left[\frac{\kappa}{\kappa^2 + (\omega - \omega_m)^2} + \frac{\kappa}{\kappa^2 + (\omega + \omega_m)^2} \right]. \quad (\text{A32})$$

We note that in general $\tilde{J}_{\text{eff}}(\omega) \neq J_{\text{eff}}(\omega)$ and hence we cannot write $L_L(t)$ as a function of a single spectral density as in Eq. (A5), in general. Yet, from our considerations in the previous section we expect that for appropriate parameters

$$\tilde{J}_{\text{eff}}(\omega) \approx J_{\text{eff}}(\omega) \quad (\text{A33})$$

such that we obtain the form of $L(t)$ in Eq. (A5) as for a macroscopic environment.

In Fig. 4 we compare the left and right hand sides of Eq. (A33) for the parameters we use in the previous section and the main text, i.e. $\omega_m/2\pi = 100\text{kHz}$, $\kappa/2\pi = 1.25\text{kHz}$ and $\bar{n}(\omega_m) = 0.025$ ($\hbar\beta = 5.91 \cdot 10^{-6}\text{s}$) where we found very good agreement between the correlation functions $L(t)$ and $L_L(t)$ (see Fig. 2). Panel **a**) shows $J_{\text{eff}}(\omega)$ (solid line) and $\tilde{J}_{\text{eff}}(\omega)$ (circles) for low frequencies and part **b**) shows the behavior around the resonance $\omega_m/2\pi = 100\text{kHz}$. Both parts of the figure show that we obtain very good agreement in frequency space, too. Part **c**) of the figure shows the relative error

$$e_J = \frac{|\tilde{J}_{\text{eff}}(\omega) - J_{\text{eff}}(\omega)|}{J_{\text{eff}}(\omega)} \quad (\text{A34})$$

which is remarkably small over the whole range $\omega/2\pi = 0 - 150\text{kHz}$. Note that the increase in the relative error for higher frequencies is because the spectral density goes to zero more rapidly than the effective one. However, since both contributions are small the effect of this difference should be negligible.

Thus, we confirm the result of the previous section: for appropriate choices of mode frequency, cooling rate and temperature, the damped oscillator evolving according to the Lindblad equation can be attributed the effective spectral density $J_{\text{eff}}(\omega)$ of a macroscopic oscillator environment. Note that the treatment is not perturbative in the spin-motion coupling λ , so that this equivalence is valid for arbitrary values of λ .

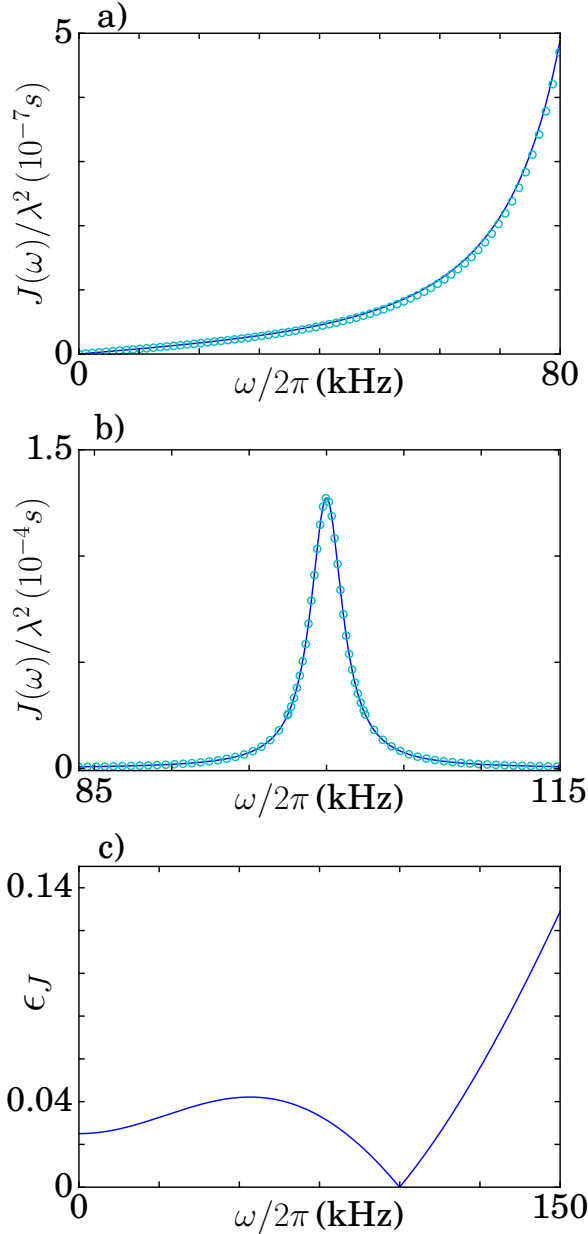


Figure 4: The figure compares $J_{\text{eff}}(\omega)$ (solid line) and $\tilde{J}_{\text{eff}}(\omega)$ (circles) from Eq. (A33) for $\omega_m/2\pi = 100\text{kHz}$, $\kappa/2\pi = 1.25\text{kHz}$ and $\bar{n} = 0.025$. Part **a**) shows the behavior for small frequencies while part **b**) depicts the two functions around the resonance $\omega_m/2\pi = 100\text{kHz}$. In part **c**) we show the relative error ϵ_J from Eq. (A34) over the relevant frequency range covered by the spectral density.

Appendix B: tDMRG simulations using the TEDOPA algorithm

For macroscopic environments the Hamiltonian for the spin-boson model considered in this work becomes

$$H = H_{\text{sys}} + H_{\text{env}} + H_{\text{int}}, \quad (\text{B1})$$

$$H_{\text{sys}} = \frac{\epsilon}{2} \sigma^z - \frac{\hbar\Delta}{2} \sigma^x, \quad (\text{B2})$$

$$H_{\text{env}} = \hbar \int_0^{\omega_{\text{max}}} d\omega \omega a_{\omega}^{\dagger} a_{\omega}, \quad (\text{B3})$$

$$H_{\text{int}} = -\sigma^z \frac{\hbar}{2} \int_0^{\omega_{\text{max}}} d\omega h(\omega) (a_{\omega} + a_{\omega}^{\dagger}), \quad (\text{B4})$$

where we have introduced a hard cutoff ω_{max} . The spectral density $J(\omega)$ is given by

$$J(\omega) = \pi h^2(\omega). \quad (\text{B5})$$

To simulate the evolution of the spin-boson model, we resorted to the Time Evolving density matrix with orthogonal polynomials (TEDOPA) algorithm. In this section we briefly present the TEDOPA scheme and refer to [5, 6] for a more detailed presentation of the algorithm. TEDOPA is a certifiable and numerically exact method to treat open quantum system dynamics [6, 7].

In a two-stage process TEDOPA first employs a unitary transformation reshaping the spin-boson model into a one-dimensional configuration. New oscillators with creation and annihilation operators b_n^{\dagger} and b_n are defined using the unitary transformations $U_n(\omega)$

$$U_n(\omega) = h(\omega) p_n(\omega), \quad (\text{B6})$$

$$b_n^{\dagger} = \int_0^{\omega_{\text{max}}} d\omega U_n(\omega) a_{\omega}^{\dagger}, \quad (\text{B7})$$

where $p_n(\omega)$, $n = 0, 1, \dots$ are orthogonal polynomials with respect to the measure $d\mu(\omega) = h^2(\omega) d\omega$ [5]. While in certain cases it is possible to perform this transformation analytically [5], in general a numerically stable procedure is used [8]. This transformation maps the environment to a semi-infinite one-dimensional chain of oscillators with nearest-neighbor interactions. In this configuration the spin only interacts with the first site of the chain. The Hamiltonian (B1) becomes

$$H = H_{\text{sys}} - \hbar \frac{t_0}{2} \sigma^z (b_0 + b_0^{\dagger}) + \sum_{n=0}^{\infty} \hbar \omega_n b_n^{\dagger} b_n + \sum_{n=0}^{\infty} \hbar t_n (b_n^{\dagger} b_{n+1} + b_n b_{n+1}^{\dagger}). \quad (\text{B8})$$

The nearest-neighbor geometry as well as coefficients ω_n and t_n are directly related to the recurrence coefficients of the three-term recurrence relation defining the orthogonal polynomials $p_n(\omega)$ [5]. This transformation from the spin-boson model to a one-dimensional geometry is depicted in Fig. 5.

In the second step this emerging configuration is treated by the Time Evolving Block Decimation (TEBD) method. TEBD generates a high fidelity approximation of the time

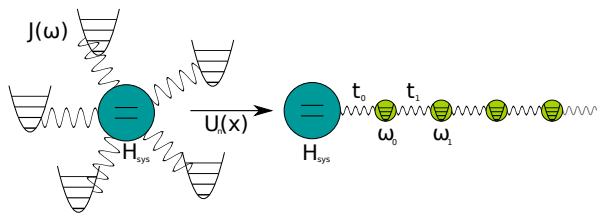


Figure 5: Illustration of the spin-boson model’s transformation into a one-dimensional configuration where the system is only coupled to the environment’s first site.

evolution of a one-dimensional system subject to a nearest-neighbor Hamiltonian with polynomially scaling computational resources. TEBD does so by dynamically restricting the exponentially large Hilbert space to its most relevant subspace thus rendering the computation feasible [9, 10]. TEBD is essentially a combination of an MPS description for a one-dimensional quantum system and an algorithm that applies two-site gates that are necessary to implement a Suzuki-Trotter time evolution. Together with MPS operations such as the application of measurements this yields a powerful simulation framework. An extension to mixed states is possible by introducing a matrix product operator (MPO) to describe the density matrix, in complete analogy to an MPS describing a state [10]. Such an extension is needed in our simulations in order to build the thermal state of the oscillator chain.

A last step is necessary to adjust this configuration further to suit numerical needs. The number of levels for the environment oscillators is restricted to a value d_{\max} to reduce the required computational resources. A suitable value for d_{\max} is related to the sites average occupation which, in turn, depends on the environment structure and temperature. In our simulations we set $d_{\max} = 5$: this value provides converged results for all examples provided. The Hilbert space dynamical reduction performed by TEBD is determined to the *bond dimension*. The optimal choice of this parameter depends on the amount of long range correlations in the system. For all the simulations used in this work, a bond dimension $\chi = 200$ provided converged results. At last, we observe that the mapping described above produces a semi-infinite chain that must be truncated in order to enable simulations. In order to avoid unphysical back-action on the system due to finite-size effects, i.e. reflections from the end of the chain, the chain has to be sufficiently long to completely give the appearance of a “large” reservoir. These truncations can be rigorously certified by analytical bounds [7]. For the examples provided in the paper, chains of $n = 15$ sites are enough to avoid boundary effects. In order to further optimize our simulations, we augmented our TEDOPA code with a Reduced-Rank Randomized Singular Value Decomposition (RRSVD) routine [11]. Singular value decomposition (SVD) is at the heart of the dimensionality reduction TEBD relies on. RRSVD is a randomized version of the SVD that provides an improved-scaling SVD, with the same accuracy as the standard state-of-the-art deterministic SVD routines.

In order to benchmark the quality of the effective model

presented in the main text we compared the dynamics of the full spin-boson model in Eq. (B1) with spectral density as in Eq. (5) of the main text with those of a spin coupled to a damped harmonic oscillator in Lindblad description. In the latter case the system evolves according to Eq. (8) of the main text with $H = H_{\text{sb1}}$ from Eq. (13) of the main text. As in the main text we chose the parameters $\varepsilon = 0$, $\kappa/2\pi = 1.25\text{kHz}$ and $\omega_m/2\pi = 100\text{kHz}$ while we considered a spin-mode coupling strength $\lambda/2\pi = 100\text{kHz}$ and set the hard cutoff in Eq. (B3) to $\omega_{\max}/2\pi = 200\text{kHz}$. We simulated the dynamics of $\langle\sigma^z(t)\rangle$ for initial product states $|\uparrow\rangle\langle\uparrow| \otimes \rho_\beta$ where ρ_β is a thermal state at inverse temperature $\hbar\beta = 5.91 \cdot 10^{-6}\text{s}$ for the macroscopic environment and a thermal state of a single mode of frequency ω_m with mean occupation $\bar{n}(\omega_m) = 0.025$ for the Lindblad case.

The results for spin energies of $\Delta/2\pi = 50, 100\text{kHz}$ are shown in Fig. 6. For both cases one can appreciate very good agreement between the two dynamics. This also shows that the correspondence to the macroscopic environment holds away from the environmental resonance $\omega_m/2\pi = 100\text{kHz}$.

Note that the simulation of one curve for the case $\Delta/2\pi = 50\text{kHz}$ takes 15 days with 16 cores on the bwForCluster JUSTUS such that simulations for the case $\Delta/2\pi = 3\text{kHz}$ presented in the main text are out of reach.

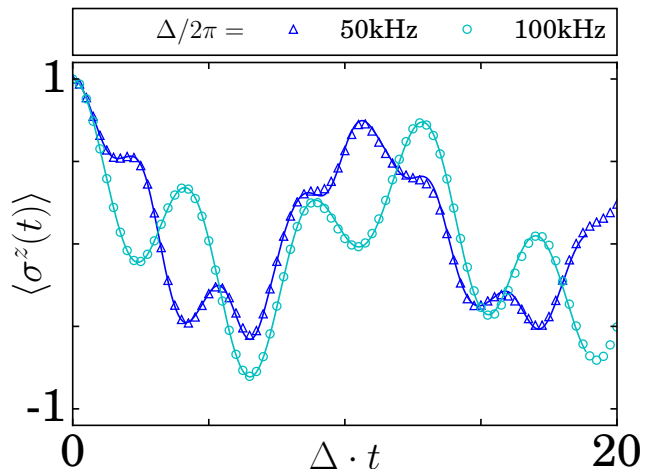


Figure 6: The figure shows the dynamics of $\langle\sigma^z(t)\rangle$ for the spin-boson Hamiltonian in Eq. (B1) with spectral density $J_{\text{eff}}(\omega)$ as in Eq. (5) of the main text (solid lines) and for a spin coupled to a damped mode described by the Lindblad equation (8) of the main text with the Hamiltonian from Eq. (13) of the main text (triangles and circles). The spin energies are $\Delta/2\pi = 100\text{kHz}$ and $\Delta/2\pi = 50\text{kHz}$. The remaining parameters are given in the text.

Appendix C: Spin-dependent optical dipole forces

In order to implement the spin-boson Hamiltonian in Eq. (13) of the main text with trapped ions we make use of the so-called spin-dependent optical dipole forces. In this section we derive the Hamiltonian for the optical dipole forces.

For clarity, we consider a somewhat simplified level structure. We employ the formalism of Ref. [12] to obtain expressions for the effective operators of a ground-state manifold weakly coupled to a decaying excited state manifold.

We consider an ion where the internal levels form a Λ -type three-level system consisting of the ground states $|\uparrow\rangle$ and $|\downarrow\rangle$ which are separated in energy by $\hbar\omega_0$ and have an electric dipole transition to a decaying excited state $|e\rangle$ (see Fig. 7). The free Hamiltonian of the system reads

$$H_{\text{at}} = \sum_{i=\downarrow,\uparrow,e} \varepsilon_i |i\rangle\langle i| \quad (\text{C1})$$

with ε_i the energy of the corresponding state. We assume that the dipole transitions are driven by two laser fields with frequencies $\omega_{1/2}$ which couple to both transitions. In a rotating wave approximation using $|\Omega_{l,s}| \ll \omega_l$ we obtain the interaction Hamiltonian

$$H_L(t) = \hbar \sum_{l=1,2} \sum_{s=\downarrow,\uparrow} \frac{\Omega_{l,s}}{2} e^{-i\omega_l t} |e\rangle\langle s| + \text{H.c.} \quad (\text{C2})$$

where $\Omega_{l,s}$ is the Rabi frequency of laser l on transition $|s\rangle \rightarrow |e\rangle$. Note that we have included the phase factors $e^{i(\mathbf{k}_l \mathbf{r} + \phi_l)}$ where \mathbf{r} denotes the ion's position and \mathbf{k}_l (ϕ_l) the laser wave vector (phase) into the Rabi frequencies. Finally, we assume that spontaneous emission from the excited level to the ground states is properly described by a dissipator in Lindblad form

$$\mathcal{D}\rho = \sum_{s=\downarrow,\uparrow} \left(L_s \rho L_s^\dagger - \frac{1}{2} \{L_s^\dagger L_s, \rho\} \right) \quad (\text{C3})$$

where $L_s = \sqrt{\Gamma_s} |s\rangle\langle e|$ and $\Gamma = \Gamma_\uparrow + \Gamma_\downarrow$ is the overall decay rate of the excited state. Putting the pieces together the system evolves according to

$$\dot{\rho} = -\frac{i}{\hbar} [H_{\text{at}} + H_L(t), \rho] + \mathcal{D}\rho. \quad (\text{C4})$$

Let us now introduce the detuning

$$\delta_{l,s} = (\varepsilon_e - \varepsilon_s) / \hbar - \omega_l \quad (\text{C5})$$

of laser l for transition $|s\rangle \rightarrow |e\rangle$. Here, we assume $\delta_{l,s} \simeq \Delta_R \gg \omega_0, \Omega_{l,s}, \Gamma$. In this case the lasers are far off resonant for all transitions such that the ground states are only weakly coupled to the excited state. We can then adiabatically eliminate the excited state from the dynamics and obtain an effective dynamics in the ground state manifold. Applying the formalism of [12] to our system we obtain the effective Lindblad equation

$$\dot{\rho} = -\frac{i}{\hbar} [H_{\text{eff}}, \rho] + \sum_k \left(L_k^{\text{eff}} \rho (L_k^{\text{eff}})^\dagger - \frac{1}{2} \{ (L_k^{\text{eff}})^\dagger L_k^{\text{eff}}, \rho \} \right). \quad (\text{C6})$$

The effective Hamiltonian H_{eff} has three contributions $H_{\text{eff}} = H_g + H_{\text{sr}} + H_{\text{odf}}$. The first part contains the shifted ground state levels

$$H_g = \sum_s (\varepsilon_s + \Delta\varepsilon_s) |s\rangle\langle s| \quad (\text{C7})$$

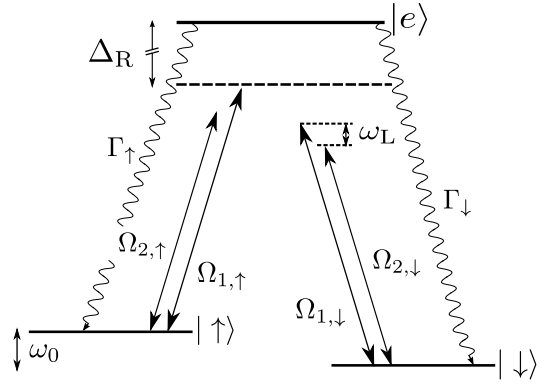


Figure 7: The figure shows a three level Λ -system consisting of the ground states $|\downarrow\rangle$ and $|\uparrow\rangle$ which are separated in frequency by ω_0 and both feature a dipole-allowed transition to the decaying excited state $|e\rangle$. The transitions are driven by two lasers and $\Omega_{l,s}$ denotes the Rabi frequency of laser l on transition $|s\rangle \rightarrow |e\rangle$. Δ_R is roughly the detuning of the lasers from the excited state. Depending on the effective laser frequency $\omega_L = \omega_1 - \omega_2$ different operations on the ground states can be implemented (see text). Spontaneous emission from the excited to the ground states happens at rates Γ_s and is indicated by the curly lines.

where the $\Delta\varepsilon_s$ are the ac-Stark shifts of the spin-levels due to the applied laser beams

$$\Delta\varepsilon_s = - \sum_{l,s} \hbar \frac{|\Omega_{l,s}|^2 \delta_{l,s}}{4\delta_{l,s}^2 + \Gamma^2}. \quad (\text{C8})$$

The second part, H_{sr} , describes two-photon stimulated Raman transitions between the spin states where a photon is absorbed from one laser beam followed by stimulated emission into the other beam

$$H_{\text{sr}} = \hbar \sum_{l',l} \frac{\Omega_{l',l}^{\text{sr}}}{2} \sigma^+ e^{-i(\omega_{l'} - \omega_l)t} + \text{H.c.} \quad (\text{C9})$$

Here, we have introduced $\sigma^+ = |\uparrow\rangle\langle\downarrow| = (\sigma^-)^\dagger$ and

$$\Omega_{l',l}^{\text{sr}} = - \frac{\Omega_{l',\uparrow}^* \Omega_{l,\downarrow} (\delta_{l',\downarrow} + \delta_{l,\uparrow})}{(2\delta_{l',\downarrow} - i\Gamma)(2\delta_{l,\uparrow} + i\Gamma)}. \quad (\text{C10})$$

The third part of the effective Hamiltonian is a time-dependent ac-Stark shift that can be used to create the optical dipole force

$$H_{\text{odf}} = \hbar \sum_s \frac{\Omega_s}{2} e^{i(\omega_1 - \omega_2)t} |s\rangle\langle s| + \text{H.c.} \quad (\text{C11})$$

where

$$\Omega_s = - \frac{\Omega_{1,s}^* \Omega_{2,s} (\delta_{2,s} + \delta_{1,s})}{(2\delta_{2,s} - i\Gamma)(2\delta_{1,s} + i\Gamma)}. \quad (\text{C12})$$

The Hamiltonian H_{odf} can be written in terms of $\sigma^z = |\uparrow\rangle\langle\uparrow| - |\downarrow\rangle\langle\downarrow|$ such that we obtain

$$H_{\text{odf}} = \hbar \frac{\Omega_{\text{rw}}}{2} e^{-i(\omega_1 - \omega_2)t} \mathbb{1} + \hbar \frac{\Omega_{\text{odf}}}{2} e^{-i(\omega_1 - \omega_2)t} \sigma^z + \text{H.c.} \quad (\text{C13})$$

where have introduced the Rabi frequencies

$$\Omega_{\text{odf}} = \frac{1}{2}(\Omega_{\uparrow}^* - \Omega_{\downarrow}^*), \quad \Omega_{\text{rw}} = \frac{1}{2}(\Omega_{\uparrow}^* + \Omega_{\downarrow}^*). \quad (\text{C14})$$

Thus, we obtain three effects on the spin states. The first is an ac-Stark shift of the spin levels due to the laser fields. The differential ac-Stark shift between spin levels can usually be canceled in experiments by adjusting polarization and intensity of the lasers [13]. Hence, we ignore this contribution. Alternatively, it could be absorbed into ω_0 .

If one chooses the frequency difference between lasers close to the transition frequency between the spin states $\omega_1 - \omega_2 \approx \omega_0$ the second part of the Hamiltonian is resonant and one can drive coherent two-photon stimulated Raman transitions between the spin states. In this case, we usually have $\Omega_{\text{odf}}, \Omega_{\text{rw}} \ll \omega_0$, the third contribution H_{odf} is highly off-resonant and can be neglected in a rotating wave approximation.

Finally, there is the regime of the spin-dependent optical dipole forces where the beatnote between the two lasers matches one of the motional frequencies $\omega_1 - \omega_2 \approx \omega_k$. Usually $\omega_k \ll \omega_0$ such that now the stimulated Raman processes in H_{sr} are highly off-resonant and can be neglected in a rotating wave approximation. Hence, in this regime we arrive at the effective Hamiltonian

$$H_{\text{eff}} = \hbar \frac{\omega_0}{2} \sigma^z + \left(\hbar \frac{\Omega_{\text{odf}}}{2} e^{i(\mathbf{k}_L \mathbf{r} + \phi_L)} e^{-i\omega_L t} \sigma^z + \text{H.c.} \right) \quad (\text{C15})$$

with the effective laser frequency $\omega_L = \omega_1 - \omega_2$ and phase $\phi_L = \phi_1 - \phi_2$. Furthermore, we have written the phases $e^{i\mathbf{k}_L \mathbf{r}}$ explicitly again and introduced the effective laser wave vector $\mathbf{k}_L = \mathbf{k}_1 - \mathbf{k}_2$. Note that we have omitted the first part of H_{odf} in Eq. (C13). For our choice of laser frequency this term would couple to the motion but it can be canceled choosing the appropriate laser intensities, polarizations and detunings [13].

Let us turn to the dissipative part. The effective Lindblad operators are found to read:

$$L_{\downarrow}^{\text{eff}} = \sqrt{\Gamma_{\downarrow}} \left(\frac{\Omega_{1,\downarrow} e^{-i\omega_1 t}}{2\delta_{1,\downarrow} - i\Gamma} + \frac{\Omega_{2,\downarrow} e^{-i\omega_2 t}}{2\delta_{2,\downarrow} - i\Gamma} \right) |\downarrow\rangle\langle\downarrow| \\ + \sqrt{\Gamma_{\downarrow}} \left(\frac{\Omega_{1,\uparrow} e^{-i\omega_1 t}}{2\delta_{1,\uparrow} - i\Gamma} + \frac{\Omega_{2,\uparrow} e^{-i\omega_2 t}}{2\delta_{2,\uparrow} - i\Gamma} \right) |\downarrow\rangle\langle\uparrow|, \quad (\text{C16})$$

$$L_{\uparrow}^{\text{eff}} = \sqrt{\Gamma_{\uparrow}} \left(\frac{\Omega_{1,\uparrow} e^{-i\omega_1 t}}{2\delta_{1,\uparrow} - i\Gamma} + \frac{\Omega_{2,\uparrow} e^{-i\omega_2 t}}{2\delta_{2,\uparrow} - i\Gamma} \right) |\uparrow\rangle\langle\uparrow| \\ + \sqrt{\Gamma_{\uparrow}} \left(\frac{\Omega_{1,\downarrow} e^{-i\omega_1 t}}{2\delta_{1,\downarrow} - i\Gamma} + \frac{\Omega_{2,\downarrow} e^{-i\omega_2 t}}{2\delta_{2,\downarrow} - i\Gamma} \right) |\uparrow\rangle\langle\downarrow|. \quad (\text{C17})$$

By keeping only the dominant contributions, i.e. those parts of the action of the Lindblad operators that are time-independent, and using $\delta_{l,s} \simeq \Delta_R$ we obtain effective operators

$$L_{\uparrow\uparrow} = \frac{1}{2} \sqrt{\Gamma_{\uparrow}} \sum_l \frac{|\Omega_{l,\uparrow}|^2}{4\Delta_R^2} \sigma^z, \quad L_{\downarrow\downarrow} = \frac{1}{2} \sqrt{\Gamma_{\downarrow}} \sum_l \frac{|\Omega_{l,\downarrow}|^2}{4\Delta_R^2} \sigma^z \quad (\text{C18})$$

and

$$L_{\uparrow\downarrow} = \sqrt{\Gamma_{\uparrow}} \sum_l \frac{|\Omega_{l,\downarrow}|^2}{4\Delta_R^2} \sigma^+, \quad L_{\downarrow\uparrow} = \sqrt{\Gamma_{\downarrow}} \sum_l \frac{|\Omega_{l,\uparrow}|^2}{4\Delta_R^2} \sigma^-. \quad (\text{C19})$$

The first two terms describe Rayleigh scattering where the spin state is not altered upon a scattering event but can introduce dephasing. The other operators describe Raman scattering where the spin state is changed upon a scattering event. If we assume the modulus of the Rabi frequencies is approximately equal $|\Omega_{l,s}| \approx \Omega_0$, we can estimate the effective scattering rate $\Gamma_{\text{eff}} \approx \Gamma \Omega_L / \Delta_R$ where $\Omega_L = \Omega_0^2 / (2\Delta_R)$ is the approximate effective laser Rabi frequency. Hence, decoherence can be largely suppressed if we choose Δ_R large enough.

Appendix D: Spin-boson Hamiltonian with trapped ions

In this section we want to show how to obtain the spin-boson Hamiltonian in Eq. (13) of the main text in an ion trap experiment. For definiteness we chose to consider a $^{24}\text{Mg}^+ - ^{25}\text{Mg}^+$ crystal. $^{25}\text{Mg}^+$ has electronic hyperfine ground states with total angular momentum $F = 2, 3$ for the valence electron in the $^2S_{1/2}$ state whose degeneracy can be lifted by a magnetic field. A possible choice for a qubit are the states $|F = 3, m_F = 3\rangle \equiv |\downarrow\rangle$ and $|F = 2, m_F = 2\rangle \equiv |\uparrow\rangle$. The hyperfine splitting between the $F = 2$ and $F = 3$ states is about $\omega_0 / 2\pi \simeq 1.8 \text{ GHz}$. At a magnetic field $B = 4 \text{ G}$ the other hyperfine states are well-separated from the qubit states due to the Zeeman interaction and we can assume the Hamiltonian

$$H_s = \hbar \frac{\omega_0}{2} \sigma^z \quad (\text{D1})$$

for the internal levels of $^{25}\text{Mg}^+$ where $\sigma^z = |\uparrow\rangle\langle\uparrow| - |\downarrow\rangle\langle\downarrow|$.

The two ions interact through their Coulomb interaction and their motion is coupled. If the ions are sufficiently cold they form a so-called Coulomb crystal and perform only small oscillations about equilibrium. We assume trapping conditions such that the ions form a string along z and their equilibrium positions read $\mathbf{r}_j^0 = (0, 0, z_j^0)^T$. Their motion is then conveniently described in terms of normal modes [14, 15]. For a crystal of N ions we obtain N modes in each direction such that, taking into account the coupled harmonic motion, the system's Hamiltonian becomes

$$H_0 = \hbar \frac{\omega_0}{2} \sigma^z + \sum_{\alpha, n} \hbar \omega_{\alpha, n} a_{\alpha, n}^\dagger a_{\alpha, n}. \quad (\text{D2})$$

Here, $\omega_{\alpha, n}$ is the frequency of mode n in direction α and $a_{\alpha, n}^\dagger$ ($a_{\alpha, n}$) creates (annihilates) an excitation in the corresponding mode. $^{24}\text{Mg}^+$ is used to sympathetically cool the ions' coupled motion. Since the internal levels are adiabatically eliminated in the description of laser cooling [16, 17] we have omitted them here. The spin transition can be driven either directly by a microwave or in a two-photon stimulated-Raman configuration (see previous section). We adopt the convention that we will call the field driving the spin transition the "microwave" independent of the physical realization.

Let us now assume the spin is driven by a microwave with frequency ω_d and Rabi frequency Ω_d and we apply a spin-dependent force as in Eq. (C15). The interaction Hamiltonian

then reads

$$H_{\text{int}} = \hbar \frac{\Omega_{\text{d}}}{2} \sigma^+ e^{-i\omega_{\text{d}}t} + \hbar \frac{\Omega_{\text{odf}}}{2} e^{i(\mathbf{k}_{\text{L}}\mathbf{r} + \phi_{\text{L}})} e^{-i\omega_{\text{L}}t} \sigma^z + \text{H.c.} \quad (\text{D3})$$

where we have set the microwave phase to zero and performed a rotating wave approximation. Ω_{odf} denotes the effective laser Rabi frequency, ω_{L} , \mathbf{k}_{L} and ϕ_{L} the effective laser frequency, wave vector and phase. We assume $\mathbf{k}_{\text{L}} = k\mathbf{e}_z$ such that the laser only couples to the motion along z . We have $\mathbf{r}_{jz} = z_j^0 + z_j$ where the z_j can be written in terms of the quantized normal modes [15]:

$$z_j = \sum_n \tilde{M}_{jn} \sqrt{\frac{\hbar}{2m_j\omega_n}} (a_n + a_n^\dagger) \quad (\text{D4})$$

where m_j is the mass of ion j , \tilde{M}_{jn} the amplitude of motional mode n at ion j in mass-weighted coordinates and $\omega_n = \omega_{z,n}$ (for the operators accordingly). The full Hamiltonian of the system then reads

$$H = H_0 + H_{\text{int}}. \quad (\text{D5})$$

Moving to an interaction picture with respect to $\tilde{H}_0 = \hbar(\omega_{\text{d}}/2)\sigma^z + \hbar\sum_{\alpha,n}\omega_{\alpha,n}a_{\alpha,n}^\dagger a_{\alpha,n}$ we obtain the transformed interaction Hamiltonian

$$\tilde{H}_{\text{int}} = \hbar \frac{\delta}{2} \sigma^z + \hbar \frac{\Omega_{\text{d}}}{2} \sigma^x + \left(\hbar \frac{\tilde{\Omega}_{\text{odf}}}{2} e^{i\sum_n \eta_n (a_n e^{-i\omega_n t} + a_n^\dagger e^{i\omega_n t})} e^{-i\omega_{\text{L}}t} \sigma^z + \text{H.c.} \right) \quad (\text{D6})$$

where $\delta = \omega_0 - \omega_{\text{d}}$, $\tilde{\Omega}_{\text{odf}} = \Omega_{\text{odf}} e^{i(kz_2^0 + \phi_{\text{L}})}$ and we have introduced the Lamb-Dicke factors $\eta_n = \tilde{M}_{2n} k \sqrt{\hbar/(2m_2\omega_n)}$. Note that we have assumed that the $^{25}\text{Mg}^+$ ion is located at site 2.

Usually for an optical wave vector $\eta_n \ll 1$ such that we can expand the exponential to first order in the η_n . In the axial direction the two-ion crystal features an in- and out-of-phase mode of motion that are well separated in frequency. More precisely, we consider a trapping potential such that a single $^{24}\text{Mg}^+$ has a center-of-mass frequency $\omega_{\text{m}}/2\pi = 2.54\text{MHz}$. The in- and out-of-phase mode frequencies of the $^{24}\text{Mg}^+ - ^{25}\text{Mg}^+$ crystal are then given by $\omega_1/2\pi = 2.51\text{MHz}$ and $\omega_2/2\pi = 4.36\text{MHz}$, respectively. If we choose the laser frequency close to the out-of-phase mode frequency $\omega_{\text{L}} \approx \omega_2$ and $\Omega_{\text{odf}} \ll 2\omega_{\text{L}}$, $\eta_1 \Omega_{\text{odf}} \ll |\omega_1 - \omega_{\text{L}}|$ we can neglect all terms except the coupling to the out-of-phase mode in a rotating wave approximation and arrive at the final Hamiltonian

$$\tilde{H}_{\text{int}} = \hbar \frac{\delta}{2} \sigma^z + \hbar \frac{\Omega_{\text{d}}}{2} \sigma^x + \left(\hbar i \eta_2 \frac{\tilde{\Omega}_{\text{odf}}}{2} a_2^\dagger \sigma^z e^{i\delta_{\text{m}}t} + \text{H.c.} \right) \quad (\text{D7})$$

where $\delta_{\text{m}} = \omega_2 - \omega_{\text{L}} \ll \omega_2$ is the detuning of the laser from the out-of-phase mode and we choose ω_{L} such that $\delta_{\text{m}} > 0$. Finally, we can cast the above Hamiltonian in a time-independent form and we recover Eq. (13) of the main text

$$\tilde{H}_{\text{int}}/\hbar = \frac{\delta}{2} \sigma^z + \frac{\Omega_{\text{d}}}{2} \sigma^x - \frac{\lambda}{2} (a_2 + a_2^\dagger) \sigma^z + \omega_{\text{m}} a_2^\dagger a_2 \quad (\text{D8})$$

where $\lambda = -i\eta_2 \tilde{\Omega}_{\text{odf}}$ can always be taken to be real and $\delta_{\text{m}} = \omega_{\text{m}}$. Thus, the mode frequency in our simulation is given by the detuning of the spin dependent force. Making the substitutions $\hbar\delta = \varepsilon$ and $\Omega_{\text{d}} = -\Delta$ we obtain the spin-boson Hamiltonian for a single mode.

Note that experimentally a finite bias ε can easily be included by introducing a detuning to the field driving the spin transition. For the spin-motion coupling we consider one has to take care that the laser beams providing the spin-motion coupling are sufficiently detuned such that the simulation is not compromised by errors due to photon scattering (see previous section). In order to avoid this source of error one could also rotate the spin basis and provide spin-motion coupling e.g. by a Mølmer-Sørensen interaction [18].

Appendix E: Computation of non-Markovianity measures

There are several different ways to define non-Markovian dynamics. Here, we start by reviewing the definition presented in [19]. Let us consider a quantum system whose time evolution is described by a completely positive and trace preserving dynamical map \mathcal{E}_{t,t_0} . Then for an initial state $\rho(t_0)$ the system's state at a later time $t \geq t_0$ is given by

$$\rho(t) = \mathcal{E}_{t,t_0} \rho(t_0). \quad (\text{E1})$$

According to [19] the dynamical map describes a Markovian evolution if and only if the map \mathcal{E}_{t_2,t_1} exists and is completely positive for all $t_2 \geq t_1 \geq t_0$. The degree of non-Markovianity of a dynamics over an interval I , \mathcal{N}_{RHP} , is then obtained by quantifying the departure of \mathcal{E}_{t_2,t_1} from complete positivity over that interval. In particular, we have

$$\mathcal{N}_{\text{RHP}} = \frac{\int_{I, \bar{g}>0} \bar{g}(t) dt}{\int_{I, \bar{g}>0} \chi[\bar{g}(t)] dt} \quad (\text{E2})$$

where the integral extends over those subintervals of I where $\bar{g}(t) > 0$. The function $\chi[x] = 1$ for $x > 0$ and $\chi[x] = 0$ else and by definition "0/0" = 0. The function $\bar{g}(t)$ is given by $\bar{g}(t) = \tanh[g(t)]$ where

$$g(t) = \lim_{\varepsilon \rightarrow 0^+} \frac{\|[\mathcal{E}_{t+\varepsilon,t} \otimes \mathbb{1}]|\psi\rangle\langle\psi|\|_1 - 1}{\varepsilon} \quad (\text{E3})$$

where $\|\dots\|_1$ denotes the trace norm and $|\psi\rangle = \frac{1}{\sqrt{d}} \sum_{n=1}^d |n,n\rangle$ is a maximally entangled state of the open system of finite dimension d with an ancillary system of the same size. Note that we restrict our considerations to finite dimensional open systems. $[\mathcal{E}_{t+\varepsilon,t} \otimes \mathbb{1}]|\psi\rangle\langle\psi|$ is the so-called Choi matrix and is positive if and only if $\mathcal{E}_{t+\varepsilon,t}$ is completely positive. Note that $g(t)$ vanishes if $\mathcal{E}_{t+\varepsilon,t}$ is completely positive. Thus, for a Markovian dynamics $g(t) = 0$ for all times and \mathcal{N}_{RHP} evaluates to zero.

We evaluated \mathcal{N}_{RHP} numerically for the spin-boson system consisting of a spin coupled to a damped mode described by Eq. (8) of the main text with the Hamiltonian in Eq. (13). To this end we divide the time interval $I = [0, T]$ that we want to inspect for non-Markovian dynamics in N equally

spaced discrete times t_i ($t_0 = 0, t_N = T$) and compute the time evolution of the basis states $|k\rangle\langle j|$, $k, j = \uparrow, \downarrow$ for all t_i . By writing the time-evolved states $|k\rangle\langle j|(t_i) = \rho_{kj}(t_i)$ as a vector $v_{kj}(t_i) = [\rho_{kj,\uparrow\uparrow}(t_i), \rho_{kj,\uparrow\downarrow}(t_i), \rho_{kj,\downarrow\uparrow}(t_i), \rho_{kj,\downarrow\downarrow}(t_i)]^T$ we can write the dynamical map $\mathcal{E}(t, t_0)$ in matrix representation

$$E(t, t_0) = [v_{\uparrow\uparrow}(t), v_{\uparrow\downarrow}(t), v_{\downarrow\uparrow}(t), v_{\downarrow\downarrow}(t)]. \quad (\text{E4})$$

The matrix for the time evolution from t_1 to t_2 where $t_2 \geq t_1 \geq t_0$ is then computed by

$$E(t_2, t_1) = E(t_2, t_0)E^{-1}(t_1, t_0) \quad (\text{E5})$$

where $E^{-1}(t_1, t_0)$ is the normal matrix inverse. The Choi matrix $[\mathcal{E}_{t_2, t_1} \otimes \mathbb{1}]|\Psi\rangle\langle\Psi|$ is proportional to the reshuffled matrix $E^R(t_2, t_1)$ of the matrix $E(t_2, t_1)$ [20]. In particular, the Choi matrix is given by

$$[\mathcal{E}_{t_2, t_1} \otimes \mathbb{1}]|\Psi\rangle\langle\Psi| = \frac{1}{d}E^R(t_2, t_1) \quad (\text{E6})$$

where d is the dimension of the finite dimensional open quantum system. For the case of a spin $E^R(t_2, t_1)$ reads

$$E^R(t_2, t_1) = \begin{pmatrix} E_{11} & E_{12} & E_{21} & E_{22} \\ E_{13} & E_{14} & E_{23} & E_{24} \\ E_{31} & E_{32} & E_{41} & E_{42} \\ E_{33} & E_{34} & E_{43} & E_{44} \end{pmatrix}. \quad (\text{E7})$$

where E_{mn} corresponds to entry m, n of the 4×4 matrix $E(t_2, t_1)$. Now, in order to obtain \mathcal{N}_{RHP} we evaluated a discrete version of $g(t)$ according to

$$g(t_i) = \frac{\|[\mathcal{E}_{t_{i+1}, t_i} \otimes \mathbb{1}]|\Psi\rangle\langle\Psi|\|_1 - 1}{t_{i+1} - t_i} = \frac{\|\frac{1}{d}E^R(t_{i+1}, t_i)\|_1 - 1}{t_{i+1} - t_i}. \quad (\text{E8})$$

The difficulty in evaluating $g(t_i)$ is to decide which values of the numerator count as zero and which are counted as finite. The numerical calculations were performed using Python's Numpy and Scipy libraries. The oscillator's Hilbert space was truncated at a maximal phonon number $n_{\text{max}} = 15$. The states were evolved in time by vectorizing the Lindblad equation and applying the matrix exponential of the Liouvillian on the vectorized form of the density matrix using the `scipy.sparse.linalg.expm_multiply` routine. For a number of parameters the resulting density matrices were compared to the density matrices obtained by performing the matrix exponential first with `scipy.sparse.linalg.expm` and then the matrix vector multiplication. For all of the spin basis states the resulting matrices typically showed trace distances of a few times 10^{-16} . Summing the largest errors of all the basis states yielded a few times 10^{-15} . Taking this value as a rough estimate of the numerical precision we set $g(t) = 0$ if the numerator was smaller than 10^{-14} . Finally, \mathcal{N}_{RHP} in this numerical

approximation is given by

$$\mathcal{N}_{\text{RHP}} = \frac{\sum_{i=1}^N \mathbb{1}_{g(t_i) > 0} \tanh[g(t_i)]}{N_{g(t_i) > 0}} \quad (\text{E9})$$

where $N_{g(t_i) > 0}$ is the number of events where $g(t_i) > 0$. For the ‘‘ohmic’’ case ($\Delta/2\pi = 3$ kHz) we chose $T = 0.01/\Delta$ and $N = 10^4$ and for the resonant case ($\Delta/2\pi = 100$ kHz) $T = 0.1/\Delta$ and $N = 10^4$. Note that taking a too small time steps eventually leads to discontinuous behavior in \mathcal{N}_{RHP} .

The computation of the measure of non-Markovianity \mathcal{N}_{BLP} [21] is somewhat easier. \mathcal{N}_{BLP} was originally proposed as a measure of non-Markovianity based on the monotonicity of the trace distance under completely positive and trace preserving evolutions and is given by

$$\mathcal{N}_{\text{BLP}} = \max_{\rho_{1/2}} \int_{I, \sigma > 0} \sigma(t) dt \quad (\text{E10})$$

where $\sigma(t) = \frac{d}{dt} D(\mathcal{E}_{t, t_0} \rho_1, \mathcal{E}_{t, t_0} \rho_2)$ and $D(\cdot, \cdot)$ is the trace distance. The integral extends over those subintervals of I where $\sigma(t) > 0$. Thus, \mathcal{N}_{BLP} detects non-Markovianity of a dynamical map \mathcal{E}_{t, t_0} if the trace distance between two initial states ρ_1 and ρ_2 increases in the course of the dynamics induced by \mathcal{E}_{t, t_0} . A nonzero value of \mathcal{N}_{BLP} can be associated with a backflow of information from the environment to the system [21]. It is known that optimal state pairs ρ_1, ρ_2 that saturate the maximum in Eq. (E10) are orthogonal and lie on the boundary of state space [22]. However, since we only want to witness non-Markovian dynamics we do not need to perform the maximization in Eq. (E10). Therefore, we can provide a useful lower bound on \mathcal{N}_{BLP} by computing the measure for the eigenstates $|\uparrow/\downarrow\rangle$, $|\pm\rangle_x$ and $|\pm\rangle_y$ of the Pauli matrices σ^z , σ^x and σ^y , respectively.

For the numerical computation of \mathcal{N}_{BLP} we considered the whole interval $[0, 20/\Delta]$. As in the previous case we considered $N = 10^4$ equally spaced points t_i in the interval and computed the time evolution for the spin starting in each of the eigenstates of the Pauli matrices. We then computed the discrete version of \mathcal{N}_{BLP}

$$\mathcal{N}_{\text{BLP}} = \sum_{i, D_{i+1} - D_i > 0} (D_{i+1} - D_i) \quad (\text{E11})$$

for each pair of eigenstates. Here the sum runs over those i where the term in brackets is larger than zero and $D_{t_i} = D(\mathcal{E}_{t_i, t_0} \rho_1, \mathcal{E}_{t_i, t_0} \rho_2)$. We note that due to the finite number of ‘‘measurements’’ there will be small deviation to the true value of \mathcal{N}_{RHP} [23]. The values shown in Fig. 2 of the main text are obtained for the initial spin states $\rho_s(0) = |\pm\rangle\langle\pm|_x$ in the Ohmic case and $\rho_s(0) = |\uparrow\rangle\langle\uparrow|, |\downarrow\rangle\langle\downarrow|$ in the resonant case.

[1] U. Weiss, *Quantum Dissipative Systems* (World Scientific, Singapore, 2007), Third Edition.

[2] A. Garg, J. N. Onuchic, and V. Ambegaokar, *Effect of friction on electron transfer in biomolecules*. J. Chem. Phys. **83**, 4491

- (1985).
- [3] H. Grabert, U. Weiss, and P. Talkner, *Quantum Theory of the Damped Harmonic Oscillator*. Z. Phys. B - Condensed Matter **55**, 87 (1984).
- [4] P. Talkner, *The failure of the Quantum Regression Hypothesis*. Ann. Phys. **167**, 390 (1986).
- [5] A. Chin, A. Rivas, S. F. Huelga, and M. B. Plenio, *Exact mapping between system-reservoir quantum models and semi-infinite discrete chains using orthogonal polynomials*. J. Math. Phys. **51**, 092109 (2010).
- [6] J. Prior, A. W. Chin, S. F. Huelga, and M. B. Plenio, *Efficient Simulation of Strong System-Environment Interactions*. Phys. Rev. Lett. **105**, 050404 (2010).
- [7] M. P. Woods, M. Cramer, and M. B. Plenio, *Simulating Bosonic Baths with Error Bars*. Phys. Rev. Lett. **115**, 130401 (2015).
- [8] W. Gautschi, *Algorithm 726: ORTHPOL—A Package of Routines for Generating Orthogonal Polynomials and Gauss-type Quadrature Rules*. ACM Trans. Math. Softw. **20**, 21 (1994).
- [9] G. Vidal, *Efficient Simulation of One-Dimensional Quantum Many-Body Systems*. Phys. Rev. Lett. **93**, 040502 (2004).
- [10] U. Schollwöck, *The density-matrix renormalization group in the age of matrix product states*. Ann. Phys. **326**, 96 (2011).
- [11] D. Tamascelli, R. Rosenbach, and M. B. Plenio, *Improved scaling of time-evolving block-decimation algorithm through reduced-rank randomized singular value decomposition*, Phys. Rev. E. **91**, 063306 (2015).
- [12] F. Reiter and A. S. Sørensen, *Effective operator formalism for open quantum systems*. Phys. Rev. A **032111** (2012).
- [13] D. J. Wineland, M. Barrett, J. Britton, J. Chiaverini, B. De-Marco, W. M. Itano, B. Jelenković, C. Langer, D. Leibfried, V. Meyer, T. Rosenband, and T. Schaetz, *Quantum information processing with trapped ions*, Phil. Trans. R. Soc. Lond. A **361**, 1349 (2003)
- [14] D. F. V. James, *Quantum dynamics of cold trapped ions with application to quantum computation* Appl. Phys. B **66**, 181 (1998)
- [15] G. Morigi and H. Walther, *Two-species Coulomb chains for quantum information*. Eur. Phys. J. D **13**, 261 (2001).
- [16] J. I. Cirac, R. Blatt, P. Zoller, and W. D. Phillips, *Laser cooling of trapped ions in a standing wave*. Phys. Rev. A **46**, 2668 (1992).
- [17] G. Morigi, *Cooling atomic motion with quantum interference*. Phys. Rev. A **67**, 033402 (2003).
- [18] A. Sørensen, and K. Mølmer, *Quantum Computation with Ions in Thermal Motion*. Phys. Rev. Lett. **82**, 1971 (1999).
- [19] A. Rivas, S. F. Huelga, M. B. Plenio, *Quantum non-Markovianity: characterization, quantification and detection*. Rep. Prog. Phys. **77**, 094001 (2014).
- [20] K. Zyczkowski, and I. Bengtsson *On duality between quantum maps and quantum states*, (arXiv:quant-ph/0401119) Open Syst. Inf. Dyn. **11**, 3-42 (2004)
- [21] H.-P. Breuer, E.-M. Laine, J. Piilo, and B. Vacchini, *Colloquium: Non-Markovian dynamics in open quantum systems*. Rev. Mod. Phys. **88**, 021002 (2016).
- [22] S. Wißmann, A. Karlsson, E.-M. Laine, J. Piilo, and H.-P. Breuer, *Optimal state pairs for non-Markovian quantum dynamics*. Phys. Rev. A **86**, 062108 (2012)
- [23] M. Wittemer, G. Clos, H.-P. Breuer, U. Warring, and T. Schaetz, *Probing Quantum Memory Effects with High Resolution*, arXiv:1702.07518